Performance Boost of a Collective Qutrit Refrigerator

Dmytro Kolisnyk[1,2] and Gernot Schaller[2,*]

[1]*Jacobs University Bremen, Campus Ring 1, Bremen 28759 , Federal Republic of Germany*

[2]*Helmholtz-Zentrum Dresden-Rossendorf, Bautzner Landstraße 400, Dresden 01328, Federal Republic of Germany*

A single qutrit with transitions selectively driven by weakly coupled reservoirs can implement one of the world's smallest refrigerators. We analyze the performance of N such fridges that are collectively coupled to the reservoirs. We observe a quantum boost, made manifest in a quadratic scaling of the steady-state cooling current with N. As N grows further, the scaling reduces to linear, since the transitions responsible for the quantum boost become energetically unfavorable. Fine-tuned interqutrit interactions may be used to maintain the quantum boost for all N and also for not perfectly collective scenarios.

I. INTRODUCTION

Beyond foundational questions, the study of quantum systems is nowadays driven by applications of quantum computation [1]. While, for these, background noise [2] is usually detrimental, it can also be turned into something useful by considering energy-conversion processes [3]. The ability of quantum systems to act as energy filters between reservoirs has fostered the whole field of quantum thermodynamics, leading to numerous applications [4]. One of the most pressing questions in this area is whether quantum heat engines can outperform their classical counterparts in some aspects [5–8].

Already, on a much simpler setting, the collective super-radiant evolution of quantum many-body systems [9–11] is an example where quantum systems can easily surpass the speed of classical ones. This can, for example, be exploited in the collective charging of quantum batteries [12–14]. Also, finite-stroke quantum thermodynamic cycles have been analyzed with collective quantum working fluids [15–23]. These mimic classical thermodynamic cycles such as, e.g., the quantum Otto cycle [24,25] and thereby depend on classical control parameters. Experimentally, such cycle implementations require a high degree of control that should not open additional decoherence channels and at present dwarfs the work that can be extracted (see, e.g., Ref. [26]). The study of autonomously operated thermodynamic cycles [27–30] is so far limited to rather low-dimensional systems, as it requires an understanding of nonlinear dynamics.

In contrast, continuously operating heat engines [31] operate while simultaneously coupled to two or more reservoirs at all times. Examples of such devices are thermoelectric generators [32–35] or quantum absorption refrigerators (QARs) [36,37]. With regard to collective effects, the latter are particularly interesting [38], as QARs require only reservoirs without particle exchange, for which superradiance is well established. Proposals [39–41] and actual realizations [42] for QARs exist and collective couplings have also been implemented experimentally in the past [43–45]. Therefore, in a previous work [46], a superradiant QAR constructed from interacting qubits has been analyzed. While superradiant cooling performance could be observed at steady state, the device required fine-tuned interactions between the qubits throughout and the preparation of an entangled initial state.

In this paper, we consider a simpler realization based on qutrits that—at least in the simplest variant—need not interact directly and do not require an entangled initial state. We start by introducing the model in Sec. II. We then explain the methods in Sec. III and discuss our results in Sec. IV, before concluding in Sec. V. For the interested reader, technical background information is provided in the appendixes. Throughout the paper, we use units with $\hbar = 1$ and $k_B = 1$, plot only dimensionless quantities, use an overbar to denote steady-state quantities, use bold symbols to refer to the interaction picture, and use $\{\hat{A}, \hat{B}\} = \hat{A}\hat{B} + \hat{B}\hat{A}$ to denote the anticommutator.

II. MODEL

Our generic starting point is a total Hamiltonian of the form

$$\hat{H} = \hat{H}_S + \sum_\nu \hat{S}^\nu \otimes \hat{B}^\nu + \sum_\nu \hat{H}_B^\nu, \qquad (1)$$
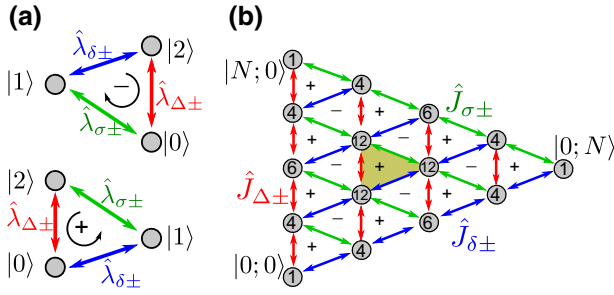
*g.schaller@hzdr.de

(a)

(b)

FIG. 1. (a) Three-level cyclic systems performing refrigeration ($N = 1$, even cycle in the lower panel and odd cycle with the work and cold reservoirs exchanged in the upper panel). (b) For larger qutrit numbers (here, $N = 4$), the 3^N states are composed in total of $N!/[(N - M - m)!M!m!]$ states (numbers inside circles) with M large (along red arrows) and m small (along blue arrows) excitations such that $0 \leq m + M \leq N$. Ordering the eigenstates in layers by the eigenvalue of Casimir operators, the largest layer corresponds to the subset of permutationally completely symmetric states, which hosts $(N + 1)(N + 2)/2$ states. Subspaces of permutationally nonsymmetric states can be grouped in additional layers (see Fig. 6) such that collective couplings then admit only intralayer transitions.

which is composed of a system part $\hat{H}_S$, different reservoirs $\hat{H}_B^\nu$, and the corresponding interactions, written as products of bath operators $\hat{B}^\nu$, that couple to different system operators $\hat{S}^\nu$. In this paper, we consider three reservoirs $\nu \in \{c, h, w\}$ that we label the cold, hot, and work (hottest) reservoirs, respectively. These reservoirs are modeled by standard harmonic oscillator baths $\hat{H}_B^\nu = \sum_k \omega_{k\nu} \hat{b}_{k\nu}^\dagger \hat{b}_{k\nu}$ throughout.

An introductory example for the system could be a single three-level model (qutrit) with ground state $|0\rangle$, first excited state $|1\rangle$, and most excited state $|2\rangle$, for which we could write $\hat{H}_S = \Delta |2\rangle \langle 2| + \delta |1\rangle \langle 1|$, where $\Delta > \delta > 0$ are the excitation energies and we gauge the ground-state energy to zero. We consider the case where the coupling between the system and the reservoir drives the individual system transitions exclusively, e.g., for the single qutrit via $\hat{S}^c = [|0\rangle \langle 1| + |1\rangle \langle 0|]$, $\hat{S}^h = [|0\rangle \langle 2| + |2\rangle \langle 0|]$, and $\hat{S}^w = [|1\rangle \langle 2| + |2\rangle \langle 1|]$ [cf. Fig. 1(a), lower panel]. In the appropriate regime (reservoirs held in thermal states with inverse temperatures obeying $\beta_c > \beta_h > \beta_w$ and the cooling condition $\beta_h \Delta > \beta_w (\Delta - \delta) + \beta_c \delta$), the single-qutrit model implements a quantum absorption refrigerator (QAR), a device that implements stochastic cooling by, on average, absorbing heat from the coldest (c) and hottest (w) reservoirs and dumping the waste heat into the intermediate-temperature (h) reservoir. We provide more details on the working principles of this configuration and also for the case where the work and cold reservoirs are exchanged [as in Fig. 1(a), upper panel] in Appendix A.

In this paper, as the system we instead consider N identical qutrits

$$\hat{H}_S = \Delta \hat{N}_\Delta + \delta \hat{N}_\delta, \quad (2)$$

where $\hat{N}_\Delta = \sum_{i=1}^N (|2\rangle \langle 2|)_i$ and $\hat{N}_\delta = \sum_{i=1}^N (|1\rangle \langle 1|)_i$ count the total number of large and small excitations present in the system and the introductory example is reproduced for $N = 1$. The reservoirs are assumed to drive individual transitions as before but the coupling to the ith qutrit may, in principle, depend on its position. Thus, we assume, as system coupling operators, the multiqutrit operators

$$\hat{S}^c = \sum_i \left[h_i^c \left(|1\rangle \langle 0| \right)_i + \text{h.c.} \right] \equiv \hat{S}_+^c + \hat{S}_-^c,$$

$$\hat{S}^h = \sum_i \left[h_i^h \left(|2\rangle \langle 0| \right)_i + \text{h.c.} \right] \equiv \hat{S}_+^h + \hat{S}_-^h, \quad (3)$$

$$\hat{S}^w = \sum_i \left[h_i^w \left(|2\rangle \langle 1| \right)_i + \text{h.c.} \right] \equiv \hat{S}_+^w + \hat{S}_-^w,$$

where $\hat{S}_-^\nu = (\hat{S}_+^\nu)^\dagger$. The dependence of the coupling on the qutrit is encoded in the coefficients $h_i^\nu \in \mathbb{C}$ and later we denote the limit $h_i^\nu \to 1$ as the *collective limit*, for which we write $\hat{J}^\nu = \lim_{h_i^\nu \to 1} \hat{S}^\nu$ and $\hat{J}_\pm^\nu = \lim_{h_i^\nu \to 1} \hat{S}_\pm^\nu$. Analogous to permutationally invariant many-qubit systems, where one can generalize single-qubit Pauli matrices—the generators of $su(2)$— to large spin operators (for potential applications, see, e.g., Ref. [47]), we can also define the collective generalizations of the generators of $su(3)$. We denote them by subscripts,

$$\hat{J}_\alpha = \frac{1}{2} \sum_{i=1}^N \hat{\lambda}_i^\alpha, \quad (4)$$

where $\hat{\lambda}_i^\alpha$ denotes the Gell-Mann matrix $\hat{\lambda}^\alpha$ (with $1 \leq \alpha \leq 8$) acting on the ith qutrit (with $1 \leq i \leq N$). In the collective limit, we can express the system coupling operators by the large qutrit operators; specifically, we have $\hat{S}_\pm^c \to \hat{J}_\pm^c = \hat{J}_6 \pm i\hat{J}_7$, $\hat{S}_\pm^h \to \hat{J}_\pm^h = \hat{J}_4 \pm i\hat{J}_5$, and $\hat{S}_\pm^w \to \hat{J}_\pm^w = \hat{J}_1 \pm i\hat{J}_2$ (see Appendix B). To represent the problem efficiently, it is advantageous to use common eigenstates of $\hat{J}_3, \hat{J}_8$ and the collective Casimir operators of $su(3)$, such as $\hat{C}_2 = \sum_{\alpha=1}^8 \hat{J}_\alpha^2$. We provide some example states in Appendix C.

The question that we address here is whether one also can observe superradiant performance boosts [48], analogous to results for interacting qubits [38,46], for this system of noninteracting qutrits.

III. METHODS

We aim at the perturbative treatment of the system-reservoir interaction (i.e., the $\hat{B}^\nu$ operators) and a description of the system by master equations. Depending on the microscopic implementation of Eq. (1), a nonperturbative treatment may require modifications to the global Hamiltonianian [49]. As in Eq. (2), all qutrits are identical and do not interact and the transformation into the interaction picture is straightforward, as shown in Eq. (D2). This facilitates the derivation of these master equations.

First, we consider the Redfield-II master equation [50] (Lamb shift omitted; see Appendix D 1 for details):

$$
\dot{\rho} = -i\left[\hat{H}_S, \rho(t)\right]
$$
$$
+ \sum_\nu \frac{\gamma_\nu(-\Omega_\nu)}{2}\left(\left[\hat{S}^\nu_+\rho, \hat{S}^\nu\right] + \left[\hat{S}^\nu, \rho\hat{S}^\nu_-\right]\right)
$$
$$
+ \sum_\nu \frac{\gamma_\nu(+\Omega_\nu)}{2}\left(\left[\hat{S}^\nu, \rho\hat{S}^\nu_+\right] + \left[\hat{S}^\nu_-\rho, \hat{S}^\nu\right]\right), \quad (5)
$$

where $\gamma_\nu(\omega) = \Gamma_\nu(\omega)[1 + n_\nu(\omega)] \geq 0$ is the product of the reservoir spectral coupling density $\Gamma_\nu(\omega)$ and the Bose distribution $n_\nu(\omega) = [e^{\beta_\nu\omega} - 1]^{-1}$, evaluated at the system excitation frequencies $\Omega_c = \delta > 0$, $\Omega_h = \Delta > 0$, and $\Omega_w = \Delta - \delta > 0$. Since we analytically continue the spectral coupling density as an odd function $\Gamma_\nu(-\omega) = -\Gamma_\nu(+\omega)$, it follows that $\gamma_\nu(-\Omega_\nu) = \Gamma_\nu(\Omega_\nu)n_\nu(\Omega_\nu) \geq 0$. The generator in Eq. (5) need not, in general, preserve the positivity of the density matrix [2] and need not be thermodynamically consistent [51]. For example, it may not exactly conserve the sum of all stationary energy currents leaving the reservoirs for nonvanishing couplings—such artifacts are, however, of higher order than the accuracy of the Redfield approach (cf. Fig. 7 in Appendix D 1). Nevertheless, for selective systems it has been shown to approach the true quantum dynamics in the appropriate regimes very well [52,53], such that we use it as our benchmark approach here.

Second, we consider the Lindblad-Gorini-Kossakowski-Sudarshan (LGKS) master equation [54,55] (Lamb shift neglected; see Appendix D 2 for details):

$$
\dot{\rho} = -i\left[\hat{H}_S, \rho(t)\right]
$$
$$
+ \sum_\nu \gamma_\nu(+\Omega_\nu)\left[\hat{S}^\nu_-\rho\hat{S}^\nu_+ - \frac{1}{2}\left\{\hat{S}^\nu_+\hat{S}^\nu_-, \rho\right\}\right]
$$
$$
+ \sum_\nu \gamma_\nu(-\Omega_\nu)\left[\hat{S}^\nu_+\rho\hat{S}^\nu_- - \frac{1}{2}\left\{\hat{S}^\nu_-\hat{S}^\nu_+, \rho\right\}\right], \quad (6)
$$

which unconditionally preserves all density-matrix properties and is also thermodynamically consistent for nonequilibrium reservoirs [56].

Third, in the perfectly collective limit ($\hat{S}^\nu_\pm \to \hat{J}^\nu_\pm$) and for a completely symmetric initial state such as, e.g.,

$$
\left|\Psi^{\text{vac}}_{\text{rep}}\right\rangle = |0\rangle \otimes \ldots \otimes |0\rangle \equiv |0; 0\rangle, \quad (7)
$$

perfect permutational symmetry is preserved (i.e., formally, the evolution is constrained to the subspace with largest Casimir-operator eigenvalue). The other permutationally completely symmetric states of this subspace with M large and m small excitations can be obtained by acting with the collective raising operators on the vacuum state $|M; m\rangle \propto (J^h_+)^M (J^c_+)^m |0; 0\rangle$. This generates, e.g., the state with N small and no large excitations $|0; N\rangle = |1 \ldots 1\rangle$ and the state with N large and no small excitations $|N; 0\rangle = |2 \ldots 2\rangle$, and many others in between [for detailed examples, see Fig. 1(b) and Appendix C]. In particular, the states in this subspace are nondegenerate and thereby [2] their populations obey a Pauli-type rate equation of the form

$$
\dot{P}_{Mm} = \sum_{M'm'} R_{Mm,M'm'} P_{M'm'}
$$
$$
- \sum_{M'm'} R_{M'm',Mm} P_{Mm}, \quad (8)
$$

where $P_{Mm} \equiv \langle M; m| \rho |M; m\rangle$ and the transition rate from $|M'; m'\rangle$ to $|M; m\rangle$ is given by $R_{Mm,M'm'} = \sum_\nu \left[\gamma_\nu(+\Omega_\nu)\left|\langle M; m| \hat{J}^\nu_- |M'; m'\rangle\right|^2 + \gamma_\nu(-\Omega_\nu)\left|\langle M; m| \hat{J}^\nu_+ |M'; m'\rangle\right|^2\right] \geq 0$. This rate equation can be directly obtained by evaluating Eq. (6) in the fully symmetric basis $|M; m\rangle$ (for details, see Appendix D 3). As Pauli rate equations can be obtained from microscopically derived LGKS equations in special cases (they always result for nondegenerate $\hat{H}_S$, here applied to isolated subspaces), they also obey their favorable properties, made manifest, e.g., in the fact that the rates for every reservoir respect local detailed balance [57]. To obtain the coefficients in Eq. (8), we require the action of the collective ladder operators in the symmetric subspace [cf. Fig. 1(b)]. They can be evaluated by representing the symmetric subspace with two bosonic modes by means of a generalized Holstein-Primakoff transform (see Appendix E), which yields

$$
\hat{J}^h_+ |M; m\rangle = \sqrt{(N - M - m)(M + 1)} |M + 1; m\rangle,
$$
$$
\hat{J}^c_+ |M; m\rangle = \sqrt{(N - M - m)(m + 1)} |M; m + 1\rangle,
$$
$$
\hat{J}^w_+ |M; m\rangle = \sqrt{(M + 1)m} |M + 1; m - 1\rangle,
$$
$$
\hat{J}^h_- |M; m\rangle = \sqrt{(N - M - m + 1)M} |M - 1; m\rangle, \quad (9)
$$
$$
\hat{J}^c_- |M; m\rangle = \sqrt{(N - M - m + 1)m} |M; m - 1\rangle,
$$
$$
\hat{J}^w_- |M; m\rangle = \sqrt{M(m + 1)} |M - 1; m + 1\rangle.
$$

Keeping $m = 0$ and $M = j_z + N/2$ for $\hat{J}_\pm^h$, or keeping $M = 0$ and $m = j_z + N/2$ for $\hat{J}_\pm^c$, or keeping $M + m = N$ and $M - m = 2j_z$ for $\hat{J}_\pm^w$, we see that the transitions along the red, blue, or green triangle facets in Fig. 1(b), respectively, precisely reproduce the usual $su(2)$ Clebsch-Gordan coefficients of the Dicke states with $j = N/2$. Accordingly, our model also includes the Dicke superradiant relaxation of two-level systems [9,10,58] if we couple to only one reservoir. These Clebsch-Gordan coefficients are largest when $j_z = 0$ (i.e., for one green, red, or blue bath, they become maximal in the middle of the respective green, red, or blue triangle facet in Fig. 1(b). Accordingly, triangles where all coefficients are large have $m \approx M \approx N/3$. In Fig. 1(b), such a central cycle is marked (shaded) and our main findings are based on the properties of these most productive cycles.

Finally, we also use a coarse-grained rate equation [59] valid for infinite temperatures of the work reservoir $n_w(\Delta - \delta) \to \infty$ (for details, see Appendix D 4):

$$
\begin{aligned}
\dot{Q}_n &= \sum_{n'} R_{nn'}^{\text{cg}} Q_{n'} - \sum_{n'} R_{n'n}^{\text{cg}} Q_n, \\
Q_n &= \sum_{M,m} P_{Mm} \delta_{M+m,n},
\end{aligned}
\tag{10}
$$

where the mesostate probabilities Q_n are occupations of states with the total number of n (small and/or large) excitations and $\delta_{M+m,n}$ denotes a Kronecker symbol. This reduction is possible because in this limit, the transitions along the green lines in Fig. 1(b) become predominant, such that all populations connected by green transitions become identical. The nonvanishing coarse-grained transition rates then become

$$
R_{n,n+1}^{\text{cg}} = [\Gamma_c(1 + n_c) + \Gamma_h(1 + n_h)] \frac{(n+1)(N-n)}{2},
$$

$$
R_{n,n-1}^{\text{cg}} = [\Gamma_c n_c + \Gamma_h n_h] \frac{(n+1)(N+1-n)}{2},
\tag{11}
$$

where $\Gamma_\nu \equiv \Gamma_\nu(+\Omega_\nu)$ and $n_\nu \equiv n_\nu(+\Omega_\nu)$, with $0 \le n \le N-1$ in the first line and $1 \le n \le N$ in the second line, respectively. The coarse-grained rate equation provides a tremendous reduction of complexity by mapping our system for $n_w \to \infty$ to a tridiagonal rate equation and we provide analytical solutions for the cooling current in Appendix D 4.

We are predominantly aiming at the steady-state solutions to Eqs. (5), (6), (8), and (10) in nonequilibrium scenarios. While it is straightforward to evaluate the energy currents $I_{E,S}^\nu(t)$ *entering the system* from balances of the system energy $d/dt\langle \hat{H}_S \rangle = \sum_\nu I_{E,S}^\nu(t)$, we also introduce microscopically derived counting fields in Appendix D, from which we demonstrate how to obtain the energy

currents *leaving the reservoirs*, $I_E^\nu = -d/dt\langle \hat{H}_B^\nu \rangle$, and their fluctuations $S_{I_E^\nu} = d/dt\left[\langle (\hat{H}_B^\nu)^2 \rangle - \langle \hat{H}_B^\nu \rangle^2\right]$ in Appendix F.

IV. RESULTS

In the collective and steady-state limits of the fully symmetric case (where the stationary solutions of the LGKS [Eq. (6)] and Pauli [Eq. (8)] equations are identical), we can establish (see Appendix G) that the stationary currents are tightly coupled,

$$
\bar{I}_E^w = \frac{\Delta - \delta}{\delta} \bar{I}_E^c, \quad \bar{I}_E^h = -\frac{\Delta}{\delta} \bar{I}_E^c,
\tag{12}
$$

and that the N-qutrit QAR is subject to the same cooling condition as a single-qutrit QAR (see Appendix D 3):

$$
\beta_h \Delta > \beta_w(\Delta - \delta) + \beta_c \delta.
\tag{13}
$$

Together with the inherent assumption $\beta_c > \beta_h > \beta_w$, this defines an operational cooling regime. Due to the tight coupling, we only quantify the cooling current below.

Our main result, however, is that, within appropriate regimes, the collective features of our model can support a quadratic scaling of the stationary cooling current with the number of qutrits N (see Fig. 2). There, we approach the problem with methods of different complexity, such as
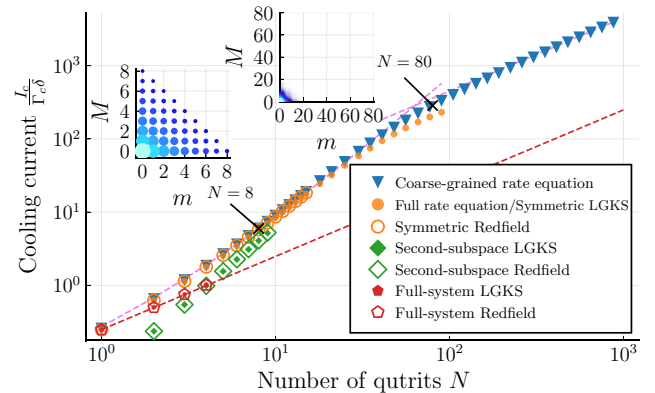

FIG. 2. A double-logarithmic plot of the dimensionless stationary energy current entering the system from the cold reservoir (cooling current) versus the number of qutrits N using different approaches and initial states (symbols; not all orange circles and blue triangles are shown). The dashed violet curves represent the analytical expressions for $n_w \to \infty$ from Eq. (D29) in the limiting cases $N \ll \bar{n}$ and $N \gg \bar{n}$. The dashed red line represents the linear cooling current scaling generated by N independent qutrits. Parameters: $\Gamma_c = \Gamma_h = \Gamma_w = 0.1\delta$, $\Delta = 10\delta$, $n_c = 10$, $n_h = 1$, and $n_w = 100$. Red pentagons correspond to averages over 100 realizations (the resulting error bars are negligibly small) with random-phase couplings such as Eq. (3) with $h_i^\nu = e^{i\varphi_i^\nu}$ and randomly distributed $\varphi_i^\nu \in [-0.1, +0.1]$.

the full Redfield treatment, the LGKS treatment, the rate-equation treatment, and the coarse-grained rate-equation treatment. We see that all methods coincide for the case $N = 1$ (bottom left), where a simple rate-equation treatment is sufficient (see Appendix A). For larger but still small N, all methods applicable for a fully collective coupling predict a faster-than-linear growth of the current with the number of qutrits N, making manifest the quantum boost of the working fluid. In Appendix H we emphasize the quantum nature of this effect. This is seen both in the LGKS (orange and green filled symbols) and the Redfield (orange and green hollow symbols) approaches. The perfect agreement of the LGKS and Redfield approaches (solid versus hollow symbols) demonstrates that in the considered weak-coupling regime, the effect is not just a consequence of the secular approximation. Furthermore, for collective couplings, we also see that the cooling current in the fully symmetric subspace [orange symbols, generated with ladder operators from the state given in Eq. (7)] is larger than that originating from a subspace with the second-largest Casimir-operator eigenvalue (green symbols), which we construct by acting with collective ladder operators $\hat{J}_{\pm}^{\nu}$ on the representative state

$$\left|\Psi_{\mathrm{rep}}\right\rangle = \frac{1}{\sqrt{N}}\Big[e^{\mathrm{i}2\pi 0/N}\left|0\ldots 01\right\rangle + e^{\mathrm{i}2\pi 1/N}\left|0\ldots 010\right\rangle$$
$$+ \ldots + e^{\mathrm{i}2\pi(N-1)/N}\left|10\ldots 0\right\rangle\Big], \qquad (14)$$

until no new orthogonal vectors are found (analogous to the discussion in Appendix C).

As one may expect for quantum features, the quadratic boost is fragile in some aspects. First, we observe, for large N, a crossover to linear scaling (filled orange circles and blue triangles), which we can link to the fact that for fixed temperatures and increasing N, the most productive cycles with $m \approx M \approx N/3$ are no longer populated significantly (the insets display stationary populations for $N = 8$ and $N = 80$). Similar inhibitions of superradiant behavior for large N have been observed elsewhere [18,60]. For the limit of an infinitely hot work reservoir (blue triangles), this can even be understood analytically (dashed magenta curves; see Appendix D 4). Second, a more severe restriction appears when we relax the assumption of collective couplings by allowing for random phases in the coupling operators (red symbols). Then, the Liouvillian no longer decouples the subspaces of different Casimir-operator eigenvalues and already, for weak deviations from the collective limit, the steady-state current no longer scales quadratically. In this limit, the steady state is close to a product of single-qutrit states (see Appendix H), such that major parts of the steady state populate less productive subspaces. When the deviations from the collective limit are small, at least two time scales will emerge: a fast one

that describes the evolution within the subspaces of constant Casimir-operator eigenvalue, while the slow one(s) will describe the leakage between the subspaces of different Casimir-operator eigenvalues. Thus, initializing the working fluid in a permutationally symmetric state such as $\left|0;0\right\rangle$ and operating the device only for a finite time, between these two time scales, may sufficiently populate states near $\left|N/3; N/3\right\rangle$ and then still yield a quantum boost. However, to stabilize the quantum enhancement at steady state and to resist small perturbations, fine-tuned interactions may be required, as exemplified at the end of this section.

To analyze the device from the thermodynamic perspective, we note that LGKS and the derived rate equations are thermodynamically fully consistent. At steady state, the first law just implies that the stationary energy currents add to zero—$\sum_{\nu}\bar{I}_E^{\nu} = 0$ [see Eq. (12)]—and the second law implies that the stationary irreversible entropy production rate is non-negative: $\bar{\sigma}_{\mathrm{i}} = -\sum_{\nu}\beta_{\nu}\bar{I}_E^{\nu} \geq 0$ [56]. As, specifically, in the symmetric subspace the currents are tightly coupled [see Eq. (12)], the coefficient of performance of the device is given by $\kappa \equiv (\bar{I}_E^c)/(\bar{I}_E^w)\Theta(\bar{I}_E^c) = \delta/(\Delta - \delta)\Theta(\bar{I}_E^c)$. One can check that in the regions of cooling functionality ($\bar{I}_E^c > 0$), the coefficient of performance is bound by its Carnot value via the condition that $\bar{\sigma}_{\mathrm{i}} \geq 0$. Tighter bounds can be obtained by considering the thermodynamic uncertainty relation [61–63],

$$\bar{\sigma}_{\mathrm{i}}\frac{\bar{S}_{I_E^{\nu}}}{(\bar{I}_E^{\nu})^2} \geq 2. \qquad (15)$$

Given the fact that all currents are tightly coupled, we use it to lower bound the fluctuations for, e.g., the cooling current as

$$\bar{S}_{I_E^c} \geq \frac{\delta \bar{I}_E^c}{\beta_h \Delta - \beta_c \delta - \beta_w(\Delta - \delta)}, \qquad (16)$$

which proves that the fluctuations inherit the superextensive scaling of the current (if present). As the eigenvalues of the Pauli rate equation cannot scale faster than N^2, we also find that the fluctuations cannot grow faster than N^2. Therefore, the relative fluctuations [64] $\sqrt{\bar{S}_{I_E^c}}/\bar{I}_E^c$ are also affected by this bound. Numerically, we find that the fluctuations approximately follow the scaling of the current. Then, it follows that these are suppressed most strongly in the regime of quadratic current and noise scaling. Due to the tight-coupling relations in Eq. (12), we find the relative fluctuations to be alike for all reservoirs [65].

Thus, if in practice one would like a device with a large cooling power, a look at Fig. 3 suggests that our device should be operated at $\beta_c \gtrsim \beta_h$. Likewise, one would like to have a device with a small product of relative fluctuations and overall entropy production, as quantified by the
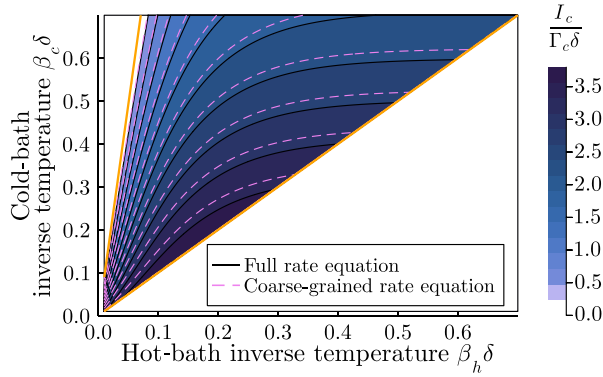
FIG. 3. A contour plot of the symmetric subspace cooling current for $N = 6$ versus the inverse dimensionless temperatures of hot $\delta\beta_h$ and cold $\delta\beta_c$ reservoirs. Cooling is achieved in the region bounded by the outer solid lines, which represent the condition given in Eq. (13). Parameters: $\Gamma_c = \Gamma_h = \Gamma_w$ and $\Delta = 10\delta$. Solid contours, $n_w = 100$; dashed contours, $n_w \to \infty$.

uncertainty quotient in Eq. (15). We find that this quotient is smallest at the other boundary of the cooling region, where $\beta_c \lessapprox \beta_h(\Delta)/\delta - \beta_w(\Delta - \delta)/\delta$ (see Fig. 4). Thus, our model recovers the usual trade-off between accuracy and performance.

By adding specifically tailored interactions to the system, we can energetically favor the maximally symmetric subspace and also the cycle with the maximum current. One example for such an interaction could be

$$\Delta\hat{H}_S = \alpha_C\left[\frac{N(N+3)}{3} - \hat{C}_2\right] + \alpha_P\left[\left(\frac{N}{3} - \hat{N}_\Delta\right)^2 + \left(\frac{N}{3} - \hat{N}_\delta\right)^2 + \left(\frac{N}{3} - \hat{N}_\Delta\right)\left(\frac{N}{3} - \hat{N}_\delta\right)\right],$$
(17)

with coefficients $\alpha_C > 0$ and $\alpha_P > 0$ penalizing the deviation from the maximum Casimir sector and the central
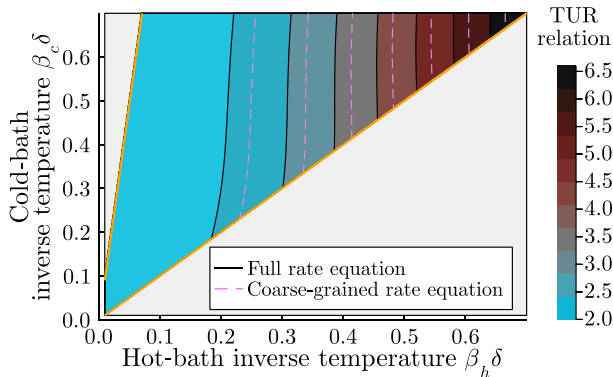

FIG. 4. A contour plot analogous to Fig. 3 but showing the thermodynamic uncertainty relation in Eq. (15) in the cooling region. Parameters as in Fig. 3.
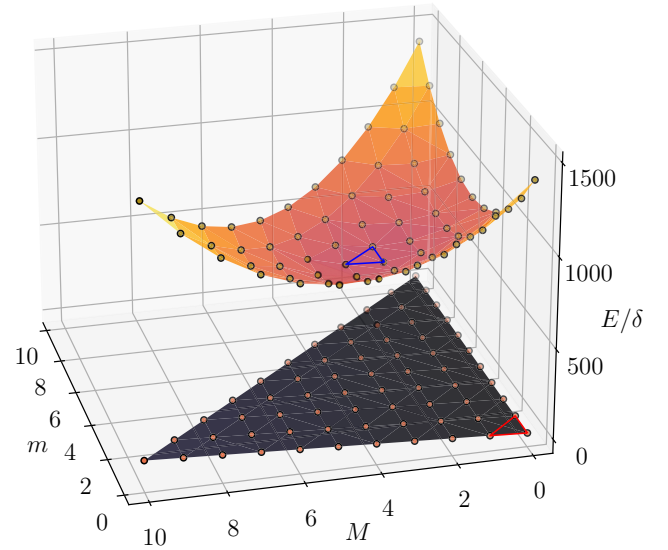

FIG. 5. A visualization of $\hat{H}_S + \Delta\hat{H}_S$ for $N = 10$ and within the maximally symmetric subspace. The bottom plane depicts the energy landscape in the absence of a penalty Hamiltonian and the energetically most favorable triangle (red) is at the lowest excitation numbers. The curved surface demonstrates the minimal penalization of the most productive triangle (blue), the plane defined by it being parallel to the plane without interactions. Parameters: $\Delta = 10\delta$ and $\alpha_P = 20\delta$ (the curved surface has been shifted upward for clarity).

triangle, respectively (all operators in square brackets are positive semidefinite). For the case where $N = 3k + 1$ with integer k (for other configurations, one may adapt the penalty Hamiltonian accordingly), the three states of the maximum-symmetry sector, $|k; k\rangle$, $|k; k + 1\rangle$, and $|k + 1; k\rangle$, have the same minimal energy penalty (see the blue triangle in Fig. 5). Therefore, it cancels out in the difference of energies and the corresponding transition rates are the same as without any interaction. Provided that the energy penalty is strong enough, $\beta_\nu\alpha_{C/P} \gg 1$, the other states with larger energy penalties can be omitted from the considerations and we obtain the current for a single QAR as discussed in Eq. (A1) but with boosted rates $\Gamma_\nu \to \Gamma_\nu\left((N + 2)/3\right)^2$, which result from the enhanced Clebsch-Gordan coefficients [see Eq. (9)] in the central cycle. Accordingly, for N qutrits, the cooling current will be boosted,

$$\bar{I}_E^{c,N} \approx \left(\frac{(N+2)}{3}\right)^2 \bar{I}_E^{c,1},$$
(18)

compared to the current from a single QAR, $\bar{I}_E^{c,1}$. As we scale all coupling constants, the fluctuations (and all higher cumulants) will increase likewise, such that both $\bar{I}_E^c \propto N^2$ and $\bar{S}_{I_E^c} \propto N^2$.

V. CONCLUSIONS

We analyze an ensemble of N identical qutrits for its suitability as a QAR using different approaches. The most striking effect is a quadratic scaling of the output (cooling current) with the number of qutrits for a permutationally symmetric configuration and collective system-reservoir couplings. This collective phenomenon can be understood analogously to the Dicke superradiant decay of two-level systems—here, put to use in an engine by means of collective couplings. In contrast to quantum computers subjected to decoherence, the performance of the QAR is only reduced to linear (classical) scaling for too large N (changing other parameters may increase the critical size) or for a not perfectly collective coupling. For nonidentical qutrits, we would expect a similar breakdown [66]. Compared to a qubit implementation [46], we want to summarize some advantages of collective qutrits. First, the initialization in the proper subspace requires just a permutationally symmetric state (no entangled states as in Ref. [46]), such as, e.g., $|0 \dots 0\rangle$. Second, to see the speed-up, we do not require fine-tuned interqutrit interactions (although they can be used to stabilize the setup against perturbations). Third, in contrast to the interacting qubit system, the (noninteracting) multiqutrit system only provides three transition frequencies, such that selective driving appears easier to implement.

On the technical side, we confirm the effect by means of a variety of methods. The use of a bosonization technique is helpful to compute the transition rates analytically. While the behavior of the collective limit can be well understood with analytical approximations and allows us to treat quite large systems, treating the non-collective limit requires significant resources. We benchmark our results by also considering the non-LGKS Redfield master equation. We find that the LGKS and Redfield results do not differ much in the considered weak-coupling regime. Beyond stronger system-reservoir coupling strengths, one may also expect larger deviations outside the tight-coupling regime, where the reservoirs no longer drive the individual transitions.

As an outlook, we think it could be interesting to consider laser-driven QARs [67,68] or investigate the fluctuations of energy currents beyond the tight-coupling regime [69] or for detuned levels [70] in greater detail. One may also be tempted to address the strong-coupling regime beyond phenomenological models [71], e.g., by using reaction coordinates [72]. This, however, should be performed while maintaining a lower spectral bound on the global Hamiltonian for all coupling strengths and values of N, in which case we expect modifications to Eq. (1) [49].

ACKNOWLEDGMENTS

APPENDIX A: A SINGLE THREE-LEVEL QAR

For the case of a single qutrit, $N = 1$, one may derive a rate equation $\dot{\vec{P}} = R\vec{P}$ for the occupation probabilities $\vec{P} = (P_0, P_1, P_2)^T$ of these states (Redfield, LGKS, and Pauli rate equations then yield the same dynamics for these probabilities).

For the normal configuration shown in Fig. 1(a, lower panel), where the cold reservoir drives transitions between the lowest two states $|0\rangle \leftrightarrow |1\rangle$, the hot between the lowest and highest $|0\rangle \leftrightarrow |2\rangle$, and the work reservoir transitions between the two excited states $|1\rangle \leftrightarrow |2\rangle$, the rate matrix becomes

$$R^+ = \begin{pmatrix} R_{00}^+ & \Gamma_c(1 + n_c) & \Gamma_h(1 + n_h) \\ \Gamma_c n_c & R_{11}^+ & \Gamma_w(1 + n_w) \\ \Gamma_h n_h & \Gamma_w n_w & R_{22}^+ \end{pmatrix}, \quad (A1)$$

where $n_v \equiv n_v(\Omega_v)$ and the negative diagonal elements are fixed by demanding vanishing of the column sums (this implements overall probability conservation). In the rate matrix, we can clearly distinguish the contributions of the individual reservoirs. From this, the energy current entering from, e.g., the cold reservoir can be obtained by standard techniques. One may compute the current via $I_E^c(t) = \sum_{ij}(E_i - E_j)R_{ij,c}^+ P_j(t)$, where $R_c^+ = R^+|_{\Gamma_h = \Gamma_w = 0}$ is the cold-reservoir rate matrix. Alternatively, one may introduce energy-counting fields $R^+ \to R^+(\chi)$ by replacing $\Gamma_c(1 + n_c) \to \Gamma_c(1 + n_c)e^{-i\delta\chi}$ and $\Gamma_c n_c \to \Gamma_c n_c e^{+i\delta\chi}$ in the off-diagonal elements of the rate matrix and compute the current via $I_E^c(t) = -i(1, 1, 1)(\partial_\chi R^+(\chi))|_{\chi=0}\vec{P}(t)$ (see also Appendix F). With this formalism, it is possible to compute also higher cumulants of the distribution of energy transfers [73]. In the limit of $n_w \to \infty$, the long-term (stationary) current reduces to

$$\bar{I}_{E+}^{c,\infty} = \frac{\Gamma_c \Gamma_h \delta(n_c - n_h)}{\Gamma_c(1 + 3n_c) + \Gamma_h(1 + 3n_h)}. \quad (A2)$$

For the case where the cold and work reservoirs are exchanged, $E_0 = 0$, $E_1 = \Delta - \delta$, and $E_2 = \Delta$, depicted in Fig. 1(a, upper panel), the rate matrix is given by

$$R^- = \begin{pmatrix} R_{00}^- & \Gamma_w(1 + n_w) & \Gamma_h(1 + n_h) \\ \Gamma_w n_w & R_{11}^- & \Gamma_c(1 + n_c) \\ \Gamma_h n_h & \Gamma_c n_c & R_{22}^- \end{pmatrix} \quad (A3)$$

and an analogous calculation leads, in the case of $n_w \to \infty$, to a slightly different cooling current:

$$\bar{I}_{E-}^{c,\infty} = \frac{\Gamma_c \Gamma_h \delta(n_c - n_h)}{\Gamma_c(2 + 3n_c) + \Gamma_h(2 + 3n_h)}. \quad (A4)$$

Both currents have the same cooling condition,

$$n_c > n_h \quad \Leftrightarrow \quad \beta_c < \beta_h \Delta/\delta, \qquad (A5)$$

which—together with $\beta_c > \beta_h$—defines an operational window for cooling the coldest reservoir. This is a sufficient and necessary condition for $n_w \to \infty$ and $N = 1$.

For finite n_w, the calculations are a bit lengthier but fully analogous. For both configurations, one obtains the sufficient and necessary cooling condition

$$\beta_w(\Delta - \delta) + \beta_c \delta < \beta_h \Delta, \qquad (A6)$$

which reduces to the previous condition as $\beta_w \to 0$. Together with the underlying assumption $\beta_c > \beta_h$, this also defines the bounds on the window of cooling for larger N (cf. Fig. 3).

APPENDIX B: COLLECTIVE SPIN REPRESENTATION

For a single qutrit, we can express the system Hamiltonian as

$$\hat{H}_S^1 = (\Delta - \delta)\frac{\hat{\lambda}^3}{2} + (\Delta + \delta)\frac{\hat{\lambda}^8}{2\sqrt{3}} + (\Delta + \delta)\frac{\mathbf{1}}{3}, \quad (B1)$$

where the $\hat{\lambda}^{3/8}$ are the two diagonal Gell-Mann matrices.

Using the collective qutrit operators given in Eq. (4), we can write the system Hamiltonian as

$$\hat{H}_S = (\Delta - \delta)\hat{J}_3 + \frac{1}{\sqrt{3}}(\Delta + \delta)\hat{J}_8 + \frac{N}{3}(\Delta + \delta)\mathbf{1}. \quad (B2)$$

Furthermore, we define collective raising and lowering operators:

$$\hat{J}_\pm^h = \sum_{i=1}^N \hat{\lambda}_{\pm,i}^h = \hat{J}_4 \pm i\hat{J}_5,$$

$$\hat{J}_\pm^c = \sum_{i=1}^N \hat{\lambda}_{\pm,i}^c = \hat{J}_6 \pm i\hat{J}_7, \qquad (B3)$$

$$\hat{J}_\pm^w = \sum_{i=1}^N \hat{\lambda}_{\pm,i}^w = \hat{J}_1 \pm i\hat{J}_2,$$

for which we find interaction-picture dynamics analogous to Eq. (D2).

In the collective limit (where $\hat{S}^\nu \to \hat{J}^\nu = \hat{J}_+^\nu + \hat{J}_-^\nu$), it follows that the quadratic and cubic Casimir operators of

the $su(3)$,

$$\hat{C}_2 = \sum_{\alpha=1}^8 \hat{J}_\alpha^2,$$

$$\hat{C}_3 = \sum_{\alpha\beta\gamma} \text{Tr}\left\{\left\{\hat{J}_\alpha, \hat{J}_\beta\right\}\hat{J}_\gamma\right\}\hat{J}_\alpha\hat{J}_\beta\hat{J}_\gamma, \qquad (B4)$$

will be automatically conserved, to all orders in the system-reservoir interaction Hamiltonian. Depending on the initial conditions, this strongly reduces the Hilbert-space dimension that needs to be treated explicitly. For example, assuming that our system is prepared, e.g., in the collective ground state of Eq. (7), we can constrain ourselves to the subspace of $(N + 1)(N + 2)/2$ permutationally symmetric states, which is significantly less demanding than treating 3^N basis states [74,75].

We label these states analogously to the maximum-angular-momentum Dicke states (known from collective two-level systems) by $|M; m\rangle$ with $0 \le M$ large and $0 \le m$ small excitations such that $0 \le M + m \le N$: specific examples are provided in Appendix C. These states are eigenstates of $\hat{N}_\Delta$ and $\hat{N}_\delta$ (or alternatively $\hat{J}_3$ and $\hat{J}_8$) and the Casimir operators. In particular, we have

$$\hat{N}_\Delta |M; m\rangle = M |M; m\rangle, \quad \hat{N}_\delta |M; m\rangle = m |M; m\rangle,$$

$$\hat{J}_3 |M; m\rangle = \left[\frac{M - m}{2}\right] |M; m\rangle,$$

$$\hat{J}_8 |M; m\rangle = \left[\frac{\sqrt{3}}{2}(M + m) - \frac{N}{\sqrt{3}}\right] |M; m\rangle, \qquad (B5)$$

$$\hat{C}_2 |M; m\rangle = \frac{N(N + 3)}{3} |M; m\rangle,$$

$$\hat{C}_3 |M; m\rangle = \frac{N(N + 3)(2N + 3)}{18} |M; m\rangle.$$

Clearly, they are also eigenstates of the system Hamiltonian $\hat{H}_S |M; m\rangle = (M\Delta + m\delta) |M; m\rangle$.

APPENDIX C: EXAMPLE STATES FOR FINITE N

In total, the Hilbert-space dimension for N qutrits is $D = 3^N$. This can be decomposed by counting the number of states with M large and m small excitations

$$N_{Nm} = \frac{N!}{(N - M - m)!M!m!}, \qquad (C1)$$

and indeed we have $3^N = \sum_{M=0}^N \sum_{m=0}^{N-M} N_{Mm}$. However, the subspace of completely symmetric states under permutations has only

$$N_{\text{symm}} = \frac{(N + 1)(N + 2)}{2} \qquad (C2)$$

elements, which are closed under the action of $\hat{J}_{\pm}^{\nu}$. This subspace is characterized by the largest Casimir-operator eigenvalues. Therefore, many states belong to subspaces that are not symmetric under permutations: see below for $N = 2$ and $N = 3$, where we adopt the convention of labeling the local eigenstates of the single-qutrit Gell-Mann matrices $\hat{\lambda}^3$ and $\hat{\lambda}^8$ as $|0\rangle$, $|1\rangle$, and $|2\rangle$.

1. Example states for $N = 2$

For $N = 2$, we have six out of the $9 = 3^2$ states in total belonging to the completely symmetric subspace

$$|0;0\rangle = |00\rangle, \quad |0;2\rangle = |11\rangle, \quad |2;0\rangle = |22\rangle,$$

$$|0;1\rangle = \frac{1}{\sqrt{2}}[|01\rangle + |10\rangle], \quad |1;0\rangle = \frac{1}{\sqrt{2}}[|02\rangle + |20\rangle],$$

$$|1;1\rangle = \frac{1}{\sqrt{2}}[|21\rangle + |12\rangle], \tag{C3}$$

and due to the complete permutational symmetry of the $\hat{J}_{\pm}^{\nu}$, the evolution of these six states is closed under collective couplings. These states are eigenstates of $\hat{C}_2$ and $\hat{C}_3$, with eigenvalues $10/3$ and $35/9$, respectively. Trivially, cyclic permutations leave these states invariant. The two-boson representation from Appendix E with $N_a = 2$ and $N_b = 0$ suffices to represent this subspace, with M and m representing the eigenvalues of $\hat{N}_\Delta$ and $\hat{N}_\delta$, respectively. One can check the action of the ladder operators in Eq. (9) among them.

Additionally, we have the three antisymmetric states

$$|\Psi_7\rangle = \frac{1}{\sqrt{2}}[|01\rangle - |10\rangle],$$

$$|\Psi_8\rangle = \frac{1}{\sqrt{2}}[|21\rangle - |12\rangle] = \hat{J}_+^h |\Psi_7\rangle, \tag{C4}$$

$$|\Psi_9\rangle = \frac{1}{\sqrt{2}}[|02\rangle - |20\rangle] = \hat{J}_+^w |\Psi_7\rangle,$$

the evolution of which is also closed under collective couplings. These states are eigenstates of the Casimir operators $\hat{C}_2$ and $\hat{C}_3$, with eigenvalues $4/3$ and $-10/9$, respectively. Cyclic permutations of the qutrits equip these states with a phase factor of $-1 = e^{i2\pi/2}$. In the four-boson representation $|M, m, Q, q\rangle$, with $N_a = 0$ and $N_b = 1$, we would identify them with the states $|\Psi_7\rangle = |0, 0, 0, 0\rangle$, $|\Psi_8\rangle = |0, 0, 1, 0\rangle$, and $|\Psi_9\rangle = -|0, 0, 0, 1\rangle$ [cf. Eq. (E2)].

2. Example states for $N = 3$

For $N = 3$, we can build the completely symmetric subspace by starting from the representative state $|\Psi_1\rangle = |0;0\rangle = |000\rangle$ (all atoms in the ground state) and we can generate, e.g.,

$$|0;1\rangle = \frac{1}{\sqrt{3}}[|001\rangle + |010\rangle + |100\rangle],$$

$$= \frac{1}{\sqrt{3}}\hat{J}_+^c |0;0\rangle,$$

$$|1;1\rangle = \frac{1}{\sqrt{6}}\big[|201\rangle + |012\rangle + |120\rangle$$

$$+ |021\rangle + |210\rangle + |102\rangle \big]$$

$$= \frac{1}{\sqrt{2}}\hat{J}_+^h |0;1\rangle,$$

$$|1;2\rangle = \frac{1}{\sqrt{3}}[|211\rangle + |112\rangle + |121\rangle]$$

$$= \frac{1}{\sqrt{2}}\hat{J}_+^c |1;1\rangle, \tag{C5}$$

and further states. In that way, we obtain $(3 + 1)(3 + 2)/2 = 10$ completely symmetric states and we can check the coefficients between them, given in Eq. (9). These are eigenstates of the Casimir operators $\hat{C}_2$ and $\hat{C}_3$, with eigenvalues 6 and 9, respectively, and can be represented by two bosonic modes $|M; m\rangle$, with $0 \leq M + m \leq N_a = N = 3$ and $N_b = Q = q = 0$. Arbitrary permutations leave these states invariant (in other words, they equip them with a phase of 1).

In addition to these, we have states with the same number of excitations as $|0;1\rangle$ but that are orthogonal to each other and also to $|0;1\rangle$. From these, we can also build further sets by acting with the ladder operators. For example, starting from $|\Psi_{11}\rangle$, which is orthogonal to $|0;1\rangle$, we obtain in total seven states,

$$|\Psi_{11}\rangle = \frac{1}{\sqrt{3}}\big[|001\rangle + e^{i2\pi/3}|010\rangle + e^{i4\pi/3}|100\rangle\big],$$

$$\hat{J}_+^c |\Psi_{11}\rangle = \frac{e^{i\pi}}{\sqrt{3}}\big[|110\rangle + e^{i\pi 2/3}|101\rangle + e^{i\pi 4/3}|011\rangle\big],$$

$$\hat{J}_+^h |\Psi_{11}\rangle = \frac{\sqrt{2}}{\sqrt{6}}\big[|201\rangle + e^{i2\pi/3}|012\rangle + e^{i4\pi/3}|120\rangle$$

$$+ |021\rangle + e^{i2\pi/3}|210\rangle + e^{i4\pi/3}|102\rangle \big],$$

$$\hat{J}_+^w |\Psi_{11}\rangle = \frac{1}{\sqrt{3}}\big[|002\rangle + e^{i2\pi/3}|020\rangle + e^{i4\pi/3}|200\rangle\big],$$

$$\hat{J}_+^h \hat{J}_+^c |\Psi_{11}\rangle = \frac{e^{i\pi}}{\sqrt{3}}\big[|112\rangle + e^{\pi i2/3}|121\rangle + e^{i\pi 4/3}|211\rangle\big],$$

$$\hat{J}_+^h \hat{J}_+^w |\Psi_{11}\rangle = \frac{e^{i\pi}}{\sqrt{3}}\big[|220\rangle + e^{i\pi 2/3}|202\rangle + e^{i\pi 4/3}|022\rangle\big],$$

$$\hat{J}_+^h \hat{J}_+^h |\Psi_{11}\rangle = \frac{2}{\sqrt{3}}\big[|221\rangle + e^{i2\pi/3}|212\rangle + e^{i4\pi/3}|122\rangle\big]. \tag{C6}$$

Cyclic permutations equip these with a phase of $e^{i2\pi/3}$. Further states can be generated when starting from $|\Psi_{18}\rangle$, which is orthogonal to $|\Psi_{11}\rangle$ and $|0;1\rangle$:

$$|\Psi_{18}\rangle = \frac{1}{\sqrt{3}}\left[|001\rangle + e^{i4\pi/3}|010\rangle + e^{i\pi 2/3}|100\rangle\right],$$

$$\hat{J}_+^c|\Psi_{18}\rangle = \frac{e^{i\pi}}{\sqrt{3}}\left(|110\rangle + e^{i\pi 4/3}|101\rangle + e^{+i\pi 2/3}|011\rangle\right),$$

$$\hat{J}_+^h|\Psi_{18}\rangle = \frac{\sqrt{2}}{\sqrt{6}}\Big[|201\rangle + e^{i\pi 4/3}|012\rangle + e^{i\pi 2/3}|120\rangle$$
$$+ |021\rangle + e^{i\pi 4/3}|210\rangle + e^{i\pi 2/3}|102\rangle\Big],$$

$$\hat{J}_+^w|\Psi_{18}\rangle = \frac{1}{\sqrt{3}}\left[|002\rangle + e^{i\pi 4/3}|020\rangle + e^{i\pi 2/3}|200\rangle\right],$$

$$\hat{J}_+^h\hat{J}_+^c|\Psi_{18}\rangle = \frac{e^{i\pi}}{\sqrt{3}}\left[|112\rangle + e^{\pi i4/3}|121\rangle + e^{+\pi i2/3}|211\rangle\right],$$

$$\hat{J}_+^h\hat{J}_+^h|\Psi_{18}\rangle = \frac{2}{\sqrt{3}}\left[|221\rangle + e^{i\pi 4/3}|212\rangle + e^{i\pi 2/3}|122\rangle\right],$$

$$\hat{J}_+^h\hat{J}_+^w|\Psi_{18}\rangle = \frac{e^{i\pi}}{\sqrt{3}}\left[|220\rangle + e^{\pi i4/3}|202\rangle + e^{\pi i2/3}|022\rangle\right].$$
$$\text{(C7)}$$

Under cyclic permutations, these obtain a phase of $e^{i4\pi/3}$. We have two additional states with exactly one small and one large excitation that are orthogonal to $|1;1\rangle$, $\hat{J}_+^h|\Psi_{11}\rangle$, and $\hat{J}_+^h|\Psi_{18}\rangle$ and to each other, and that have similar behavior under cyclic permutations. These are as follows:

$$|\Psi_{25}\rangle = \frac{1}{\sqrt{6}}\Big[|201\rangle + e^{i\pi 2/3}|012\rangle + e^{i\pi 4/3}|120\rangle$$
$$- |021\rangle - e^{i\pi 2/3}|210\rangle - e^{i\pi 4/3}|102\rangle\Big],$$

$$|\Psi_{26}\rangle = \frac{1}{\sqrt{6}}\Big[|201\rangle + e^{i\pi 4/3}|012\rangle + e^{i\pi 2/3}|120\rangle$$
$$- |021\rangle - e^{i\pi 4/3}|210\rangle - e^{i\pi 2/3}|102\rangle\Big]. \quad \text{(C8)}$$

The first one obtains a phase $e^{i2\pi/3}$ under cyclic permutations and the second the phase $e^{i4\pi/3}$. Additionally, one can see that the states $\hat{J}_+^h|\Psi_{11}\rangle$ and $\hat{J}_+^h|\Psi_{18}\rangle$ are symmetric under the state-conditional permutation $0 \leftrightarrow 2$, whereas the states $|\Psi_{25}\rangle$ and $|\Psi_{26}\rangle$ are antisymmetric. One can get to $|\Psi_{25}\rangle$, e.g., via $\hat{J}_+^w\hat{J}_+^c|\Psi_{11}\rangle$ and subsequent orthonormalization. Analogously, $|\Psi_{26}\rangle$ can be reached by $\hat{J}_+^w\hat{J}_+^c|\Psi_{18}\rangle$ and subsequent orthonormalization. Thus, the $16 = 2 \times 8$ states $|\Psi_{11}\rangle, \ldots, |\Psi_{26}\rangle$ are closed under the action of a collective reservoir: they have eigenvalues of Casimir operators $\hat{C}_2$ and $\hat{C}_3$ of 3 and 0, respectively. In the bosonic four-mode representation $|M, m, Q, q\rangle$, the eight states for this Casimir subspace and the given behavior under

cyclic permutations can be constructed from the subspaces with $N_a = 1$ and $N_b = 1$. Formally, via $(M, m), (Q, q) \in \{(0, 0), (0, 1), (1, 0)\}$, the bosonic four-mode representation yields nine (six nondegenerate and three degenerate) possible states in total but one superposition of the three degenerate states, $|0, 0, 1, 0\rangle$, $|0, 1, 0, 1\rangle$, and $|1, 0, 0, 0\rangle$ has a different Casimir-operator eigenvalue and can be decoupled.

Finally, the last state is

$$|\Psi_{27}\rangle = \frac{1}{\sqrt{6}}\Big[|012\rangle + |120\rangle + |201\rangle$$
$$- |021\rangle - |210\rangle - |102\rangle\Big]. \quad \text{(C9)}$$

It is annihilated by $\hat{J}_\pm^v$, has the smallest eigenvalue 0 of both Casimir operators $\hat{C}_i$, and is also inert under cyclic permutations. It is fully antisymmetric under the exchange of any two qutrits and it corresponds in the bosonic four-mode representation to the state $|0, 0, 0, 0\rangle$, with $N_a = 0$ and $N_b = 0$.

We note that in the collective limit, states such as $|\Psi_{27}\rangle$ remain fully inert: they are dark states [76,77]. From the combinatorics of states, we may expect dark states with $m = M = N/3$ for any number N divisible by 3. These dark states will then have minimum, i.e., vanishing, Casimir-operator eigenvalue $\langle\hat{C}_2\rangle = 0$. In particular, since the case $N = 6$ already hosts more than one dark state, superpositions of these could be used to form, e.g., a decoherence-protected logical qubit in the presence of all possible collective system-reservoir interactions.

3. States for $N = 4$

For $N = 4$, we may consider Fig. 1(b) as the largest (top) layer of all states that can be grouped in a pyramidlike structure as shown in Fig. 6.

APPENDIX D: DERIVATION OF THE EVOLUTION EQUATIONS

1. Redfield master equation

For multiple weakly coupled reservoirs, the dissipators act additively, such that for a single-coupling operator per reservoir $\hat{H}_I^v = \hat{S}^v \otimes \hat{B}^v$, the Redfield-II master equation [53] can be readily written as

$$\dot{\boldsymbol{\rho}} = -\int_0^\infty d\tau \sum_v C_v(+\tau)\left[\hat{\boldsymbol{S}}^v(t), \hat{\boldsymbol{S}}^v(t-\tau)\boldsymbol{\rho}(t)\right]$$
$$-\int_0^\infty d\tau \sum_v C_v(-\tau)\left[\boldsymbol{\rho}(t)\hat{\boldsymbol{S}}^v(t-\tau), \hat{\boldsymbol{S}}^v(t)\right], \quad \text{(D1)}$$

where we denote the interaction picture by bold symbols and introduce the reservoir correlation function $C_v(\tau) =$
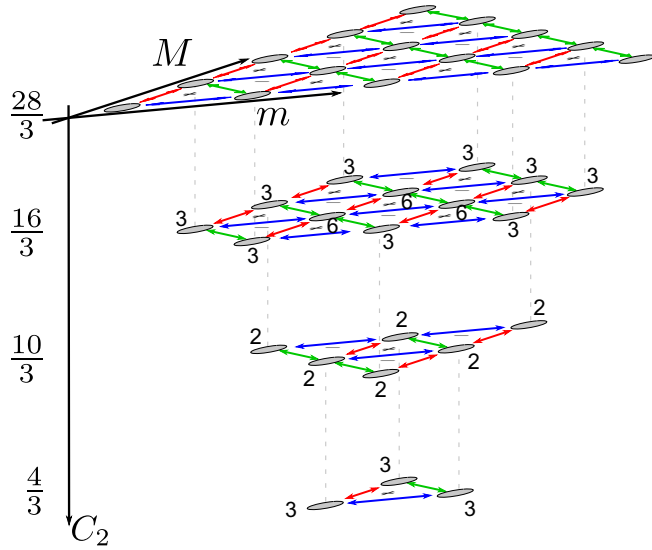
FIG. 6. A map of all $3^4 = 81$ collective basis states for $N = 4$ versus small and large numbers of excitations (horizontal directions) and versus the Casimir-operator $\hat{C}_2$ eigenvalue. The top layer corresponds to the 15 nondegenerate states from the completely permutationally symmetric subspace with the largest Casimir-operator eigenvalue, as shown in Fig. 1(b). It evolves independently from the other states for fully collective transitions. The other levels are grouped according to decreasing Casimir-operator eigenvalue, with the numbers close to the symbols indicating the degeneracy.

$\mathrm{Tr}_B\left\{e^{+i\hat{H}_B^\nu \tau}\hat{B}^\nu e^{-i\hat{H}_B^\nu \tau}\hat{B}^\nu \bar{\rho}_B^\nu\right\}$. In particular, for the noninteracting system Hamiltonian in Eq. (2) and the coupling operators in Eq. (3), the transformation into the interaction picture can be made very explicit:

$$
\begin{aligned}
e^{+i\hat{H}_S t}\hat{S}_\pm^c e^{-i\hat{H}_S t} &= e^{\pm i\delta t}\hat{S}_\pm^c, \\
e^{+i\hat{H}_S t}\hat{S}_\pm^h e^{-i\hat{H}_S t} &= e^{\pm i\Delta t}\hat{S}_\pm^h, \\
e^{+i\hat{H}_S t}\hat{S}_\pm^w e^{-i\hat{H}_S t} &= e^{\pm i(\Delta-\delta)t}\hat{S}_\pm^w.
\end{aligned} \tag{D2}
$$

Thus, writing the Redfield equation in the Schrödinger picture, we obtain (cf., e.g., Ref. [78])

$$
\begin{aligned}
\dot{\rho} = &-i\left[\hat{H}_S, \rho(t)\right] - \sum_\nu \int_0^\infty d\tau\, C_\nu(+\tau)\left[\hat{S}^\nu, \boldsymbol{\hat{S}^\nu}(-\tau)\rho(t)\right] \\
&- \sum_\nu \int_0^\infty d\tau\, C_\nu(-\tau)\left[\rho(t)\boldsymbol{\hat{S}^\nu}(-\tau), \hat{S}^\nu\right] \\
= &-i\left[\hat{H}_S, \rho(t)\right] - \sum_\nu \int_0^\infty C_\nu(+\tau)e^{-i\Omega_\nu \tau}d\tau\left[\hat{S}^\nu, \hat{S}_+^\nu \rho\right] \\
&- \sum_\nu \int_0^\infty C_\nu(+\tau)e^{+i\Omega_\nu \tau}d\tau\left[\hat{S}^\nu, \hat{S}_-^\nu \rho\right]
\end{aligned}
$$

$$
\begin{aligned}
&- \sum_\nu \int_0^\infty C_\nu(-\tau)e^{-i\Omega_\nu \tau}d\tau\left[\rho\hat{S}_+^\nu, \hat{S}^\nu\right] \\
&- \sum_\nu \int_0^\infty C_\nu(-\tau)e^{+i\Omega_\nu \tau}d\tau\left[\rho\hat{S}_-^\nu, \hat{S}^\nu\right].
\end{aligned} \tag{D3}
$$

To simplify this expression, one may express the integral prefactors by inserting the Fourier transform of the correlation function $C_\nu(\tau) = 1/2\pi \int \gamma_\nu(\omega)e^{-i\omega\tau}d\omega$ and subsequently invoking the Sokhotskij-Plemelj theorem,

$$
\frac{1}{2\pi}\int_0^\infty e^{+i\omega\tau}d\tau = \frac{1}{2}\delta(\omega) + \frac{i}{2\pi}\mathcal{P}\frac{1}{\omega}, \tag{D4}
$$

where $\mathcal{P}$ denotes the Cauchy principal value. This allows to write the integrals in terms of Hermitian (real) and anti-Hermitian (imaginary) parts, e.g.,

$$
\begin{aligned}
\int_0^\infty C_\nu(+\tau)e^{+i\Omega_\nu \tau}d\tau &= \frac{1}{2}\gamma_\nu(+\Omega_\nu) + \frac{1}{2}\sigma_\nu(+\Omega_\nu), \\
\int_0^\infty C_\nu(-\tau)e^{+i\Omega_\nu \tau}d\tau &= \frac{1}{2}\gamma_\nu(-\Omega_\nu) - \frac{1}{2}\sigma_\nu(-\Omega_\nu),
\end{aligned} \tag{D5}
$$

and analogously for the terms with $\Omega_\nu \to -\Omega_\nu$. In the above equations, the functions on the right-hand side are then the even and odd Fourier transforms of the reservoir correlation functions:

$$
\begin{aligned}
\gamma_\nu(\omega) &= \int C_\nu(\tau)e^{+i\omega\tau}d\tau, \\
\sigma_\nu(\omega) &= \int C_\nu(\tau)\mathrm{sgn}(\tau)e^{+i\omega\tau}d\tau.
\end{aligned} \tag{D6}
$$

The Lamb-shift parts $\sigma_\nu(\pm\Omega_\nu)$ are negligible in comparison to $\hat{H}_S$, such that it is common practice to neglect them. Eventually, this transforms Eq. (D3) into Eq. (5). The Redfield equation conserves trace and Hermiticity but not necessarily the positivity of the density matrix. For general operators $\hat{O}$, one can rewrite it in terms of expectation values:

$$
\begin{aligned}
\frac{d}{dt}\left\langle \hat{O}\right\rangle = &+i\left\langle\left[\hat{H}_S, \hat{O}\right]\right\rangle \\
&+ \sum_\nu \frac{\gamma_\nu(-\Omega_\nu)}{2}\Big[\left\langle\left[\hat{S}^\nu, \hat{O}\right]\hat{S}_+^\nu\right\rangle \\
&+ \left\langle\hat{S}_-^\nu\left[\hat{O}, \hat{S}^\nu\right]\right\rangle\Big] \\
&+ \sum_\nu \frac{\gamma_\nu(+\Omega_\nu)}{2}\Big[\left\langle\left[\hat{S}^\nu, \hat{O}\right]\hat{S}_-^\nu\right\rangle \\
&+ \left\langle\hat{S}_+^\nu\left[\hat{O}, \hat{S}^\nu\right]\right\rangle\Big].
\end{aligned} \tag{D7}
$$

Thus, it is easy to see that the above equation conserves all operators that commute with both $\hat{H}_S$ and $\hat{S}^\nu$, i.e., if

$[\hat{O}, \hat{H}_S] = [\hat{O}, \hat{S}^\nu] = 0$, one also has $\mathrm{Tr}\left\{\hat{O}\dot{\rho}\right\} = 0$. This is the case in the collective limit, where $\hat{S}^\nu \to \hat{J}^\nu$, e.g., for the Casimir operators $\hat{O} \to \hat{C}_i$.

Apart from the Lamb-shift terms, the spectral coupling densities of the reservoirs are always evaluated at their transition frequencies, δ, Δ, and $\Delta - \delta$, respectively. Thus, for our calculations in the main text (where the Lamb shift is neglected), the actual form of the spectral coupling density is not relevant. To confirm that the Lamb-shift contributions are indeed negligible, we employ a special model for the spectral coupling density. Using

$$\Gamma_\nu(\omega) = \Gamma_\nu \frac{\omega}{\epsilon_\nu} \frac{\delta_\nu^4}{(\omega^2 - \epsilon_\nu^2)^2 + \delta_\nu^4}, \quad \text{(D8)}$$

the correlation function $C_\nu(\tau)$ as well as the Lamb-shift contribution,

$$\sigma_\nu(\omega) = \frac{\mathrm{i}}{\pi} \mathcal{P} \int \frac{\gamma_\nu(\omega')}{\omega - \omega'} d\omega', \quad \text{(D9)}$$

may be computed analytically (although this yields extremely lengthy expressions). To compare with our calculations in the main text, we use resonant reservoirs with $\epsilon_c = \delta$, $\epsilon_h = \Delta$, and $\epsilon_w = \Delta - \delta$ and compute the Redfield current in Fig. 2 with Lamb-shift corrections included (setting $\delta_\nu = \epsilon_\nu$). For the other parameters chosen as in Fig. 2, we find the effects of the Lamb-shift contributions to be negligible.

Similar to the rate-equation discussion in Appendix A, the cold-reservoir energy current may now be computed using different options. Adopting the systems perspective, one may obtain it by computing the system energy balance from Eq. (5). The energy current entering from the cold reservoir then becomes

$$I_{E,S}^c = \frac{\Gamma_c n_c}{2} \mathrm{Tr}\left\{\hat{H}_S\left(\left[\hat{S}_+^c \rho, \hat{S}^c\right] + \left[\hat{S}^c, \rho\hat{S}_-^c\right]\right)\right\}$$
$$+ \frac{\Gamma_c(1+n_c)}{2} \mathrm{Tr}\left\{\hat{H}_S\left(\left[\hat{S}^c, \rho\hat{S}_+^c\right] + \left[\hat{S}_-^c \rho, \hat{S}^c\right]\right)\right\} \quad \text{(D10)}$$

and analogously for the other reservoirs. Alternatively, we may microscopically derive energy-counting fields [53,78,79], which adopts the perspective of energy leaving the reservoir and yields a tilted Liouvillian $\mathcal{L} \to \mathcal{L}(\chi)$. In Eq. (5), this would effectively lead to the replacements $\left(\left[\hat{S}^c, \rho\hat{S}_+^c\right] + \left[\hat{S}_-^c \rho, \hat{S}^c\right]\right) \to$ $\left(\hat{S}^c \rho\hat{S}_+^c e^{-\mathrm{i}\delta\chi} + \hat{S}_-^c \rho\hat{S}^c e^{-\mathrm{i}\delta\chi} - \rho\hat{S}_+^c \hat{S}^c - \hat{S}^c \hat{S}_-^c \rho\right)$, and the analogous one $\left(\left[\hat{S}_+^c \rho, \hat{S}^c\right] + \left[\hat{S}^c, \rho\hat{S}_-^c\right]\right) \to \left(\hat{S}_+^c \rho\hat{S}^c e^{+\mathrm{i}\delta\chi}\right.$ $\left.+ \hat{S}^c \rho\hat{S}_-^c e^{+ii\chi} - \hat{S}^c \hat{S}_+^c \rho - \rho\hat{S}_-^c \hat{S}^c\right)$. The current (and noise)
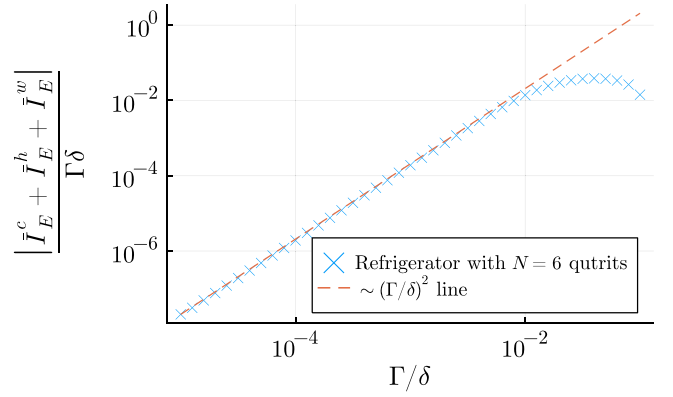

FIG. 7. A double-logarithmic plot of the sum of all stationary Redfield energy currents leaving the reservoirs versus the coupling strength Γ for $N = 6$ qutrits. The apparent violation of the first law scales as Γ^2 (dashed line), which is beyond the accuracy of the Redfield equation. Parameters: $\Gamma = \Gamma_c = \Gamma_h = \Gamma_w$, $\Delta = 10\delta$, $n_c = 10$, $n_h = 1$, and $n_w = 100$.

can then be computed using the methods in Appendix F. For the current leaving the cold reservoir, this yields

$$I_E^c = -\frac{\Gamma_c \delta(1 + n_c)}{2} \mathrm{Tr}\left\{\hat{S}^c \rho\hat{S}_+^c + \hat{S}_-^c \rho\hat{S}^c\right\}$$
$$+ \frac{\Gamma_c \delta n_c}{2} \mathrm{Tr}\left\{\hat{S}_+^c \rho\hat{S}^c + \hat{S}^c \rho\hat{S}_-^c\right\}. \quad \text{(D11)}$$

In general, we have $I_E^\nu \neq I_{E,S}^\nu$ for the Redfield equation. Moreover, while by construction the stationary currents for the system add to zero, $\sum_\nu \bar{I}_{E,S}^\nu = 0$, this is only approximately true in the Redfield approach for the energy currents leaving the reservoir. In Fig. 7, we plot the sum of energy currents leaving the reservoirs (i.e., the deviation from the first law at steady state) versus the coupling strengths to the reservoirs (assumed equal). One can see that the deviation from energy conservation becomes smaller when the coupling strength is reduced. Moreover, it scales with Γ^2 (the Redfield approach is accurate to order Γ), such that this apparent violation can be considered as a truncation artifact and does not indicate a violation of the first law in the weak-coupling regime, where, for our model, the Redfield and LGKS solutions agree.

2. Secular master equations

Under a secular approximation, Eq. (D3) simplifies to

$$\dot{\rho} \approx -\sum_\nu \int_0^\infty d\tau C_\nu(+\tau) e^{-\mathrm{i}\Omega_\nu \tau} \left[\hat{S}_-^\nu, \hat{S}_+^\nu \rho(t)\right]$$
$$- \sum_\nu \int_0^\infty d\tau C_\nu(+\tau) e^{+\mathrm{i}\Omega_\nu \tau} \left[\hat{S}_+^\nu, \hat{S}_-^\nu \rho(t)\right]$$

$$-\sum_{\nu}\int_0^\infty d\tau\, C_\nu(-\tau)e^{+i\Omega_\nu\tau}\left[\boldsymbol{\rho}(t)\hat{S}_-^\nu,\hat{S}_+^\nu\right]$$

$$-\sum_{\nu}\int_0^\infty d\tau\, C_\nu(-\tau)e^{-i\Omega_\nu\tau}\left[\boldsymbol{\rho}(t)\hat{S}_+^\nu,\hat{S}_-^\nu\right]$$

$$=-i\sum_{\nu}\left[\frac{\sigma_\nu(-\Omega_\nu)}{2i}\hat{S}_-^\nu\hat{S}_+^\nu+\frac{\sigma_\nu(+\Omega_\nu)}{2i}\hat{S}_+^\nu\hat{S}_-^\nu,\boldsymbol{\rho}\right]$$

$$+\sum_{\nu}\gamma_\nu(+\Omega_\nu)\left[\hat{S}_-^\nu\boldsymbol{\rho}\hat{S}_+^\nu-\frac{1}{2}\left\{\hat{S}_+^\nu\hat{S}_-^\nu,\boldsymbol{\rho}\right\}\right]$$

$$+\sum_{\nu}\gamma_\nu(-\Omega_\nu)\left[\hat{S}_+^\nu\boldsymbol{\rho}\hat{S}_-^\nu-\frac{1}{2}\left\{\hat{S}_-^\nu\hat{S}_+^\nu,\boldsymbol{\rho}\right\}\right]. \quad \text{(D12)}$$

Back in the Schrödinger picture, we thus have

$$\dot{\rho}=-i\left[\hat{H}_S+\sum_{\nu}\frac{\sigma_\nu(-\Omega_\nu)}{2i}\hat{S}_-^\nu\hat{S}_+^\nu+\frac{\sigma_\nu(+\Omega_\nu)}{2i}\hat{S}_+^\nu\hat{S}_-^\nu,\boldsymbol{\rho}\right]$$

$$+\sum_{\nu}\gamma_\nu(+\Omega_\nu)\left[\hat{S}_-^\nu\rho\hat{S}_+^\nu-\frac{1}{2}\left\{\hat{S}_+^\nu\hat{S}_-^\nu,\rho\right\}\right]$$

$$+\sum_{\nu}\gamma_\nu(-\Omega_\nu)\left[\hat{S}_+^\nu\rho\hat{S}_-^\nu-\frac{1}{2}\left\{\hat{S}_-^\nu\hat{S}_+^\nu,\rho\right\}\right], \quad \text{(D13)}$$

which upon neglecting the Lamb shift $\sigma_\nu(\pm\Omega_\nu)$, reduces to Eq. (6). This equation is of LGKS form and thermalizes the system when all reservoirs are at the same equilibrium temperature. Furthermore, when evaluating only the populations of ρ in the system energy eigenbasis for situations where the system Hamiltonian is nondegenerate (at least within a conserved subspace), we obtain the simple Pauli-type rate equation as exemplified in Appendix D 3.

In the collective limit, the associated effective non-Hermitian Hamiltonian,

$$H_{\text{eff}}=\hat{H}_S-\frac{i}{2}\sum_{\nu}\left[\Gamma_\nu(1+n_\nu)\hat{J}_+^\nu\hat{J}_-^\nu+\Gamma_\nu n_\nu\hat{J}_-^\nu\hat{J}_+^\nu\right], \quad \text{(D14)}$$

is diagonal in the maximum-symmetry subspace H_{eff} $|M;m\rangle=\lambda_{Mm}|M;m\rangle$. Its eigenvalues can be calculated analytically via Eq. (9) and their imaginary part—related to the waiting-time distribution [80] between any two jump events [81]—indicates that for fixed thermal reservoirs n_ν and coupling strengths Γ_ν, the waiting time is minimized for $M\approx m\approx N/3$ (maximum engine activity). Specifically, from the imaginary part of

$$\lambda_{\frac{N}{3},\frac{N}{3}}=\frac{N}{3}(\Delta+\delta)-\frac{i}{2}\frac{N}{3}\left(\frac{N}{3}+1\right)\left[\sum_{\nu}\Gamma_\nu(1+2n_\nu)\right], \quad \text{(D15)}$$

we can conclude that the lifetime of the states participating in the central cycle scales as $\tau\propto N^{-2}$.

The currents can now be computed by analogy with Sec. D 1, i.e., either by the energy flowing into the system from the cold reservoir,

$$I_{E,S}^c=\Gamma_c(1+n_c)\text{Tr}\left\{\hat{H}_S\left[\hat{S}_-^c\rho\hat{S}_+^c-\frac{1}{2}\left\{\hat{S}_+^c\hat{S}_-^c,\rho\right\}\right]\right\}$$

$$+\Gamma_c n_c\text{Tr}\left\{\hat{H}_S\left[\hat{S}_+^c\rho\hat{S}_-^c-\frac{1}{2}\left\{\hat{S}_-^c\hat{S}_+^c,\rho\right\}\right]\right\}, \quad \text{(D16)}$$

or by assessing the energy flow out of the cold reservoir with counting fields $\hat{S}_-^c\rho\hat{S}_+^c\to\hat{S}_-^c\rho\hat{S}_+^c e^{-i\delta\chi}$ and $\hat{S}_+^c\rho\hat{S}_-^c\to\hat{S}_+^c\rho\hat{S}_-^c e^{+i\delta\chi}$ and then using the methods of Sec. F. The current leaving the cold reservoir can then be obtained via $I_E^c(t)=-i\text{Tr}\left\{\mathcal{L}'(0)\vec{\rho}(t)\right\}$ and becomes

$$I_E^c=\Gamma_c\delta n_c\text{Tr}\left\{\hat{S}_+^c\rho\hat{S}_-^c\right\}-\Gamma_c\delta(1+n_c)\text{Tr}\left\{\hat{S}_-^c\rho\hat{S}_+^c\right\}. \quad \text{(D17)}$$

In contrast to the Redfield case discussed above, we find $I_E^\nu=I_{E,S}^\nu$, such that we can unambiguously write the first law of thermodynamics as

$$\frac{d}{dt}\text{Tr}\left\{\hat{H}_S\rho\right\}=\sum_{\nu}I_E^\nu(t). \quad \text{(D18)}$$

Using Spohn's inequality [82], one can also establish the second law of thermodynamics:

$$\frac{d}{dt}\text{Tr}\left\{-\rho\ln\rho\right\}-\sum_{\nu}\beta_\nu I_E^\nu(t)\ge 0. \quad \text{(D19)}$$

These equations bound the coefficient of performance of the QAR by its Carnot value.

3. Pauli rate equation

For the fully symmetric case, the derivation of a rate equation becomes particularly simple. We can formally insert a diagonal density matrix in the fully symmetric subspace

$$\rho=\sum_{M,m}P_{Mm}|M;m\rangle\langle M;m| \quad \text{(D20)}$$

into Eq. (6), which, with the help of Eq. (9), yields

$$\dot{P}_{Mm}=\gamma_c(-\delta)(N-M-m+1)mP_{M,m-1}$$

$$-\gamma_c(-\delta)(N-M-m)(m+1)P_{M,m}$$

$$+\gamma_c(+\delta)(N-M-m)(m+1)P_{M,m+1}$$

$$-\gamma_c(+\delta)(N-M-m+1)mP_{M,m}$$

$$+\gamma_h(-\Delta)(N-M-m+1)MP_{M-1,m}$$

$$-\gamma_h(-\Delta)(N-M-m)(M+1)P_{M,m}$$

$$+ \gamma_h(+\Delta)(N - M - m)(M + 1)P_{M+1,m}$$

$$- \gamma_h(+\Delta)(N - M - m + 1)MP_{M,m}$$

$$+ \gamma_w(-\Delta + \delta)M(m + 1)P_{M-1,m+1}$$

$$- \gamma_w(-\Delta + \delta)(M + 1)mP_{M,m}$$

$$+ \gamma_w(+\Delta - \delta)(M + 1)mP_{M+1,m-1}$$

$$- \gamma_w(+\Delta - \delta)M(m + 1)P_{M,m}. \quad \text{(D21)}$$

This is precisely the Pauli-type rate equation [Eq. (8)], where we note that rates outside allowed states do naturally vanish. In particular, we can identify the transitions that increase the system energy as

$$R_{(M,m+1),(M,m)} = \Gamma_c n_c \cdot (N - M - m)(m + 1),$$

$$R_{(M+1,m),(M,m)} = \Gamma_h n_h \cdot (N - M - m)(M + 1), \quad \text{(D22)}$$

$$R_{(M+1,m-1),(M,m)} = \Gamma_w n_w \cdot m(M + 1),$$

while transitions that decrease it are always a bit larger due to local detailed balance:

$$R_{(M,m),(M,m+1)} = \Gamma_c(1 + n_c) \cdot (N - M - m)(m + 1),$$

$$R_{(M,m),(M+1,m)} = \Gamma_h(1 + n_h) \cdot (N - M - m)(M + 1),$$

$$R_{(M,m),(M+1,m-1)} = \Gamma_w(1 + n_w) \cdot m(M + 1). \quad \text{(D23)}$$

Currents can be obtained by analogy with the case $N = 1$ discussed in Appendix A. One may compute them via the energy balance of the system, which, for a system subject to the rate equation $\dot{P}_i = \sum_{ij} \sum_\nu \left[R_{ij}^\nu P_j - R_{ji}^\nu P_i \right]$, with R_{ij}^ν denoting the transition rate from system energy eigenstate j to system energy eigenstate i triggered by reservoir ν, generically yields the expression $I_E^\nu = \sum_{ij}(E_i - E_j)R_{ij}^\nu P_j$. Alternatively, one may also insert counting fields (or use the ones from the LGKS description), which effectively corresponds to the replacement $\Gamma_c n_c \to \Gamma_c n_c e^{+i\delta\chi}$ and $\Gamma_c(1 + n_c) \to \Gamma_c(1 + n_c)e^{-i\delta\chi}$ in the off-diagonal matrix elements of the rate matrix and then use the methods of Appendix F. As with the previous section, these two approaches are equivalent and thermodynamically consistent.

For multiqutrit systems, the exact computation of the steady state is already cumbersome for the collective limit and the Pauli rate equation [Eq. (8)], such that we do not provide analytical results for the currents. However, in Appendix G, we perform a cycle decomposition to establish tight-coupling relations between the currents.

4. Coarse-grained rate equation

For the case where the work reservoir is infinitely hot, $n_w \to \infty$, the associated green transitions in Fig. 1 become predominant and along these transitions (with $m + M = \text{const}$) the populations become approximately equal (but

still remain conditioned on the total number of excitations). This allows us to coarse grain [59,83] the populations by summarizing all states with the same total number of excitations,

$$Q_n = \sum_{M,m} \delta_{M+m,n} P_{M,m}. \quad \text{(D24)}$$

As the states connected by work-reservoir transitions equilibrate much faster in this limit, we have, for their conditional probability,

$$\lim_{n_w \to \infty} \frac{P_{M,m}}{Q_n} \bigg|_{M+m=n} = \frac{1}{n + 1}. \quad \text{(D25)}$$

Summing over the respective states of Eq. (8) allows us to obtain a coarse-grained one-dimensional Markovian rate equation:

$$\dot{Q}_n = \sum_{M,m} \delta_{M+m,n} \bigg[\gamma_c(-\delta)(N - M - m + 1)m \frac{P_{M,m-1}}{Q_{n-1}} Q_{n-1}$$

$$- \gamma_c(-\delta)(N - M - m)(m + 1) \frac{P_{M,m}}{Q_n} Q_n$$

$$+ \gamma_c(+\delta)(N - M - m)(m + 1) \frac{P_{M,m+1}}{Q_{n+1}} Q_{n+1}$$

$$- \gamma_c(+\delta)(N - M - m + 1)m \frac{P_{M,m}}{Q_n} Q_n$$

$$+ \gamma_h(-\Delta)(N - M - m + 1)M \frac{P_{M-1,m}}{Q_{n-1}} Q_{n-1}$$

$$- \gamma_h(-\Delta)(N - M - m)(M + 1) \frac{P_{M,m}}{Q_n} Q_n$$

$$+ \gamma_h(+\Delta)(N - M - m)(M + 1) \frac{P_{M+1,m}}{Q_{n+1}} Q_{n+1}$$

$$- \gamma_h(+\Delta)(N - M - m + 1)M \frac{P_{M,m}}{Q_n} Q_n$$

$$+ \gamma_w(-\Delta + \delta)M(m + 1) \frac{P_{M-1,m+1}}{Q_n} Q_n$$

$$- \gamma_w(-\Delta + \delta)(M + 1)m \frac{P_{M,m}}{Q_n} Q_n$$

$$+ \gamma_w(+\Delta - \delta)(M + 1)m \frac{P_{M+1,m-1}}{Q_n} Q_n$$

$$- \gamma_w(+\Delta - \delta)M(m + 1) \frac{P_{M,m}}{Q_n} Q_n \bigg]$$

$$\overset{n_w \to \infty}{\approx} R_{n,n+1}^{cg} Q_{n+1} + R_{n,n-1}^{cg} Q_{n-1}$$

$$- [R_{n-1,n}^{cg} + R_{n+1,n}^{cg}]Q_n, \quad \text{(D26)}$$

where $n \in \{0, 1, \ldots, N\}$ denotes the total number of excitations and we insert the conditional probabilities. In the

coarse-grained rates, the mesostate-internal transitions due to the work reservoir cancel out, whereas the other reservoirs determine the transitions between mesostates:

$$
R_{n,n+1}^{\mathrm{cg}} = \sum_{M,m} \frac{\delta_{M+m,n}}{n+2} \Big[\Gamma_c(1+n_c)(N-M-m)(m+1)
$$

$$
+ \Gamma_h(1+n_h)(N-M-m)(M+1) \Big],
$$

$$
R_{n,n-1}^{\mathrm{cg}} = \sum_{M,m} \frac{\delta_{M+m,n}}{n} \Big[\Gamma_c n_c(N-M-m+1)m
$$

$$
+ \Gamma_h n_h(N-M-m+1)M \Big], \tag{D27}
$$

which evaluate to Eq. (11). Note that the case $R_{0,-1}^{\mathrm{cg}} = 0$ has to be treated separately, as the state with zero excitations does not need to be coarse grained. As a sanity check, we remark that for $N = 1$, the proper coarse-grained rates (which one obtains by applying an procedure analogous to the rate matrices in Sec. A) for a single QAR are reproduced. We note that the resulting effective rates for cold and hot reservoirs no longer obey local detailed balance, which allows energy to flow out of the cold reservoir. The simple tridiagonal form of this effective rate equation has the advantage that the stationary state can be computed analytically, since it obeys

$$
\bar{Q}_n = \frac{R_{n,n-1}^{\mathrm{cg}}}{R_{n-1,n}^{\mathrm{cg}}} \frac{R_{n-1,n-2}^{\mathrm{cg}}}{R_{n-2,n-1}^{\mathrm{cg}}} \cdot \ldots \cdot \frac{R_{1,0}^{\mathrm{cg}}}{R_{0,1}^{\mathrm{cg}}} \bar{Q}_0, \quad \sum_n \bar{Q}_n = 1. \tag{D28}
$$

Making the ratios explicit with Eq. (11), we can determine $\bar{Q}_0$ from the normalization condition and from that write the stationary cooling current with $\bar{n} = (\Gamma_c n_c + \Gamma_h n_h)/(\Gamma_c + \Gamma_h)$, $\alpha_{\bar{n}} = \bar{n}/(\bar{n}+1)$, and $R_{ij}^c \equiv R_{ij}^{\mathrm{cg}}|_{\Gamma_h \to 0}$:

$$
\bar{I}_E^c = \delta \sum_{n=1}^{N} R_{n,n-1}^c \bar{Q}_{n-1} - \delta \sum_{n=0}^{N-1} R_{n,n+1}^c \bar{Q}_{n+1}
$$

$$
= \frac{\Gamma_c \delta}{2} \sum_{n=0}^{N} \Big[(n+2)(N-n)n_c
$$

$$
- n(N-n+1)(1+n_c) \Big] \bar{Q}_n
$$

$$
= \frac{\Gamma_c \Gamma_h \delta}{2(\Gamma_c + \Gamma_h)} (n_c - n_h) f_N(\bar{n}),
$$

$$
f_N(\bar{n}) \equiv \frac{g_N(\bar{n}) + \alpha_{\bar{n}}^{N+1} h_N(\bar{n})}{\bar{n}+1 - \alpha_{\bar{n}}^{N+1} [2+\bar{n}+N]},
$$

$$
g_N(\bar{n}) \equiv 2(N-3\bar{n})(\bar{n}+1),
$$

$$
h_N(\bar{n}) \equiv N^2 + (5+4\bar{n})N + 6(\bar{n}+1)^2. \tag{D29}
$$

In the current, only the term $(n_c - n_h)$ can turn negative, such that we recover the original cooling condition for $n_w \to \infty$ given in Eq. (A5). Apart from that, the scaling factor $f_N(\bar{n}) > 0$ can be analyzed for various limits. First, we have $f_1(\bar{n}) = 2/(1+3\bar{n})$, which yields the same current as Eq. (A2). Second, for very large $N \gg \bar{n}$, we can drop the terms with powers of $\alpha_{\bar{n}} < 1$, such that $f_N(\bar{n}) \to 2N$, and the current will eventually just scale linearly: $\bar{I}_E^c \approx (\Gamma_c \Gamma_h \delta)/(\Gamma_c + \Gamma_h)(n_c - n_h)N$. Third, for $N \ll \bar{n}$, we have $f_N(\bar{n}) \to (N(N+3))/6\bar{n}$ and we maintain a quadratic scaling for the current: $\bar{I}_E^c \approx (\Gamma_c \Gamma_h \delta(n_c - n_h))/(12(\Gamma_c n_c + \Gamma_h n_h))N(N+3)$. The crossover system size N^* between these regimes can be found by simply equating the limits and it yields $N^* = 12\bar{n} - 3$. These limits can be seen well in Fig. 2 (dashed magenta curves). The crossover between two scaling regimes is thus quite analogous to previous results for collective qubit systems [60]. We can see that the current becomes maximal when $n_h \to 0$ (which can be reached by $\Delta \to \infty$ and then implies $n_c \to (\Gamma_c + \Gamma_h)/(\Gamma_c)\bar{n}$). Then, we can numerically maximize $(n_c - n_h)f_N(\bar{n}) \to (\Gamma_c + \Gamma_h)/(\Gamma_c)\bar{n}f_N(\bar{n})$ as a function of $\bar{n}$ only. For large N, the position of this maximum is roughly at $\bar{n} \approx N/6$ and the current scales quadratically in N at this maximum.

5. Interacting Pauli rate equation

Pauli rate equations can also be derived for interactions present in the system Hamiltonian $\hat{H}_S$. If these interactions can be expressed by the permutationally symmetric operators $\hat{C}_2$, $\hat{N}_\delta$ and $\hat{N}_\Delta$ (or, equivalently, by $\sum_\alpha \hat{J}_\alpha^2$, $\hat{J}_3$, and $\hat{J}_8$), as in Eq. (17), it follows that the same eigenstates can be used for the representation of the problem and that only the eigenvalues change. Labeling the eigenstates of $\hat{H}_S$ with the multi-index i, the Pauli rate equation will then generically have the structure [2]

$$
\dot{P}_i = \sum_\nu \sum_j \Big[R_{ij}^\nu P_j - R_{ji}^\nu P_i \Big],
$$

$$
R_{ij}^\nu = \gamma_\nu(E_j - E_i) \big| \langle i| \hat{S}^\nu |j\rangle \big|^2. \tag{D30}
$$

The inherent local detailed balance for the transition rates then exponentially suppresses excitations into undesired Casimir subspaces and undesired excitation numbers, whereas relaxation from the excited eigenvalues down to the desired most productive cycle is still possible. Thus, for $N = 3k + 1$ with integer k and sufficiently large penalty parameters $\beta_\nu \alpha_{C/P} \gg 1$, we can neglect the excited states and constrain our considerations to the states from the maximum-symmetry (Casimir) sector with $\langle \hat{C}_2 \rangle = N(N+3)/3$: $|k;k\rangle$, $|k;k+1\rangle$, and $|k+1;k\rangle$. These three states

then have the energies

$$
\begin{aligned}
E_0 &= k(\Delta + \delta) + \alpha_P/3, \\
E_1 &= k\Delta + (k+1)\delta + \alpha_P/3, \\
E_2 &= (k+1)\Delta + k\delta + \alpha_P/3,
\end{aligned}
\tag{D31}
$$

such that the penalty α_P cancels out in their differences. As the eigenstates $|M; m\rangle$ remain the same, the quadratic enhancement from Eq. (9) is preserved and we obtain the current equation [Eq. (A2)] with $\Gamma_\nu \to \Gamma_\nu ((N+2)/3)^2$, leading to the corresponding enhancement given in Eq. (18).

APPENDIX E: BOSONIZATION

The eight operators $\{\hat{J}_3, \hat{J}_8, \hat{J}_+^h, \hat{J}_-^h, \hat{J}_+^c, \hat{J}_-^c, \hat{J}_+^w, \hat{J}_-^w\}$ inherit a closed algebra from the associated single-qutrit versions:

$$
\begin{aligned}
&\left[\hat{J}_3, \hat{J}_+^h\right] = \frac{\hat{J}_+^h}{2}, \ \left[\hat{J}_3, \hat{J}_+^c\right] = -\frac{\hat{J}_+^c}{2}, \ \left[\hat{J}_3, \hat{J}_+^w\right] = \hat{J}_+^w, \\
&\left[\hat{J}_8, \hat{J}_+^h\right] = \frac{\sqrt{3}\hat{J}_+^h}{2}, \ \left[\hat{J}_8, \hat{J}_+^c\right] = \frac{\sqrt{3}\hat{J}_+^c}{2}, \\
&\left[\hat{J}_+^h, \hat{J}_-^h\right] = \sqrt{3}\hat{J}_8 + \hat{J}_3, \ \left[\hat{J}_+^c, \hat{J}_-^c\right] = \sqrt{3}\hat{J}_8 - \hat{J}_3, \\
&\left[\hat{J}_+^w, \hat{J}_-^w\right] = 2\hat{J}_3, \\
&\left[\hat{J}_+^h, \hat{J}_-^c\right] = \hat{J}_+^w, \ \left[\hat{J}_+^h, \hat{J}_+^w\right] = -\hat{J}_+^c, \\
&\left[\hat{J}_+^c, \hat{J}_+^w\right] = -\hat{J}_+^h.
\end{aligned}
\tag{E1}
$$

Other independent commutators (which do not follow from Hermitian conjugation) just vanish.

1. Four-mode Holstein-Primakoff transform

The above commutation relations can be realized with four bosonic modes with annihilation operators $\hat{a}_\Delta, \hat{a}_\delta, \hat{b}_\Delta$, and $\hat{b}_\sigma$ obeying the usual bosonic commutation relations by using a generalization [84] of the Holstein-Primakoff transform:

$$
\begin{aligned}
\hat{J}_3 &= \hat{b}_\sigma^\dagger \hat{b}_\sigma + \frac{1}{2}\hat{b}_\Delta^\dagger \hat{b}_\Delta + \frac{1}{2}\left(\hat{a}_\Delta^\dagger \hat{a}_\Delta - \hat{a}_\delta^\dagger \hat{a}_\delta\right) - \frac{N_b}{2}, \\
\hat{J}_8 &= \frac{\sqrt{3}}{2}\hat{b}_\Delta^\dagger \hat{b}_\Delta + \frac{\sqrt{3}}{2}\left(\hat{a}_\Delta^\dagger \hat{a}_\Delta + \hat{a}_\delta^\dagger \hat{a}_\delta\right) - \frac{N_a}{\sqrt{3}} - \frac{N_b}{2\sqrt{3}}, \\
\hat{J}_+^h &= \hat{a}_\Delta^\dagger \sqrt{N_a - \hat{a}_\Delta^\dagger \hat{a}_\Delta - \hat{a}_\delta^\dagger \hat{a}_\delta} \\
&\quad + \hat{b}_\Delta^\dagger \sqrt{N_b - \hat{b}_\Delta^\dagger \hat{b}_\Delta - \hat{b}_\sigma^\dagger \hat{b}_\sigma}, \\
\hat{J}_+^c &= \hat{a}_\delta^\dagger \sqrt{N_a - \hat{a}_\Delta^\dagger \hat{a}_\Delta - \hat{a}_\delta^\dagger \hat{a}_\delta} + \hat{b}_\Delta^\dagger \hat{b}_\sigma, \\
\hat{J}_+^w &= \hat{a}_\Delta^\dagger \hat{a}_\delta - \hat{b}_\sigma^\dagger \sqrt{N_b - \hat{b}_\Delta^\dagger \hat{b}_\Delta - \hat{b}_\sigma^\dagger \hat{b}_\sigma}.
\end{aligned}
\tag{E2}
$$

Here, the integer numbers $N_a \geq 0$ and $N_b \geq 0$ determine the physically admissible states, i.e., they have to be adjusted to match the behavior of the collective qutrit operators such as, e.g., the Hamiltonian:

$$
\begin{aligned}
\hat{H}_S &= \Delta \left[\hat{a}_\Delta^\dagger \hat{a}_\Delta + \hat{b}_\Delta^\dagger \hat{b}_\Delta + \hat{b}_\sigma^\dagger \hat{b}_\sigma + \frac{N - N_a - 2N_b}{3}\right] \\
&\quad + \delta \left[\hat{a}_\delta^\dagger \hat{a}_\delta - \hat{b}_\sigma^\dagger \hat{b}_\sigma + \frac{N - N_a + N_b}{3}\right].
\end{aligned}
\tag{E3}
$$

In particular, the Fock states $|M, m, Q, q\rangle$, with M, m, Q, and q denoting the eigenvalues of $\hat{a}_\Delta^\dagger \hat{a}_\Delta$, $\hat{a}_\delta^\dagger \hat{a}_\delta$, $\hat{b}_\Delta^\dagger \hat{b}_\Delta$, and $\hat{b}_\sigma^\dagger \hat{b}_\sigma$, respectively, are physically admissible when

$$
\begin{aligned}
&[(N_a = M + m) \vee (Q = 0)] \wedge \\
&[(N_b = Q + q) \vee (M = 0)] \wedge \\
&[(q = 0) \vee (m = 0)].
\end{aligned}
\tag{E4}
$$

For example, the special case $Q = q = N_b = 0$ fulfills these conditions and admits an even simpler representation of the algebra with just two bosonic modes, which we discuss below, and that corresponds to the fully symmetric subspace discussed in the main text. For the subspace with the second-largest Casimir-operator eigenvalue, one has to use the four-boson representation instead. As one always has $N_a + N_b \leq N$ and $0 \leq M + m \leq N_a$ as well as $0 \leq Q + q \leq N_b$, it follows that largest Clebsch-Gordan coefficients (and therefore the largest currents) may originate from the fully symmetric subspace.

2. Two-mode Holstein-Primakoff transform

When $Q = q = N_b = 0$, the transformation requires only two bosonic modes [76,85] with a non-negative integer N_a:

$$
\begin{aligned}
\hat{J}_3 &= \frac{1}{2}\left(\hat{a}_\Delta^\dagger \hat{a}_\Delta - \hat{a}_\delta^\dagger \hat{a}_\delta\right), \\
\hat{J}_8 &= \frac{\sqrt{3}}{2}\left(\hat{a}_\Delta^\dagger \hat{a}_\Delta + \hat{a}_\delta^\dagger \hat{a}_\delta\right) - \frac{N_a}{\sqrt{3}}, \\
\hat{J}_+^h &= \hat{a}_\Delta^\dagger \sqrt{N_a - (\hat{a}_\Delta^\dagger \hat{a}_\Delta + \hat{a}_\delta^\dagger \hat{a}_\delta)}, \\
\hat{J}_+^c &= \hat{a}_\delta^\dagger \sqrt{N_a - (\hat{a}_\Delta^\dagger \hat{a}_\Delta + \hat{a}_\delta^\dagger \hat{a}_\delta)}, \\
\hat{J}_+^w &= \hat{a}_\Delta^\dagger \hat{a}_\delta,
\end{aligned}
\tag{E5}
$$

and analogously for the lowering operators. It turns out that the fully symmetric subspace can be covered by the choice $N_a = N$ (the number of qutrits). Then, the fully symmetric states discussed in the main text are equivalent to the Fock-state representation with just two bosonic modes $|M; m\rangle \equiv |M, m, 0, 0\rangle$.

The system Hamiltonian in Eq. (E3) then simply assumes the form $\hat{H}_S = \Delta \hat{a}_\Delta^\dagger \hat{a}_\Delta + \delta \hat{a}_\delta^\dagger \hat{a}_\delta$. As a sanity check, representing the Casimir operator in terms of the bosons, we obtain the maximum eigenvalue valid for the fully symmetric subspace $\langle \hat{C}_2 \rangle = (N(N+3))/3$. From the bosonic properties, it is then straightforward to compute the Clebsch-Gordan coefficients, given in Eq. (9), of the symmetric subspace discussed in the main text.

3. Master equation for large N

The master equation given in Eq. (6) can, in the symmetric subspace and for large N such that $\langle a_\nu^\dagger a_\nu \rangle \ll N$, be simplified by expanding the roots in Eq. (E5), which yields

$$\dot{\rho} = -i \left[\Delta \hat{a}_\Delta^\dagger \hat{a}_\Delta + \delta \hat{a}_\delta^\dagger \hat{a}_\delta, \rho \right]$$

$$+ N\Gamma_c(1 + n_c) \left[\hat{a}_\delta \rho \hat{a}_\delta^\dagger - \frac{1}{2} \left\{ \hat{a}_\delta^\dagger \hat{a}_\delta, \rho \right\} \right]$$

$$+ N\Gamma_c n_c \left[\hat{a}_\delta^\dagger \rho \hat{a}_\delta - \frac{1}{2} \left\{ \hat{a}_\delta \hat{a}_\delta^\dagger, \rho \right\} \right]$$

$$+ N\Gamma_h(1 + n_h) \left[\hat{a}_\Delta \rho \hat{a}_\Delta^\dagger - \frac{1}{2} \left\{ \hat{a}_\Delta^\dagger \hat{a}_\Delta, \rho \right\} \right]$$

$$+ N\Gamma_h n_h \left[\hat{a}_\Delta^\dagger \rho \hat{a}_\Delta - \frac{1}{2} \left\{ \hat{a}_\Delta \hat{a}_\Delta^\dagger, \rho \right\} \right]$$

$$+ \Gamma_w(1 + n_w) \left[\hat{a}_\delta^\dagger \hat{a}_\Delta \rho \hat{a}_\Delta^\dagger \hat{a}_\delta - \frac{1}{2} \left\{ \hat{a}_\Delta^\dagger \hat{a}_\delta \hat{a}_\delta^\dagger \hat{a}_\Delta, \rho \right\} \right]$$

$$+ \Gamma_w n_w \left[\hat{a}_\Delta^\dagger \hat{a}_\delta \rho \hat{a}_\delta^\dagger \hat{a}_\Delta - \frac{1}{2} \left\{ \hat{a}_\delta^\dagger \hat{a}_\Delta \hat{a}_\Delta^\dagger \hat{a}_\delta, \rho \right\} \right]. \quad \text{(E6)}$$

In the absence of the work reservoir $\Gamma_w \to 0$, we find that relaxation to the steady state therefore scales with Nt,

$$\left\langle \hat{a}_\delta^\dagger \hat{a}_\delta \right\rangle_t = N_\delta^0 e^{-N\Gamma_c t} + n_c(1 - e^{-N\Gamma_c t}), \quad \text{(E7)}$$

and analogously for the hot reservoir. The above also makes manifest superradiant decay, as the relaxation time is inversely proportional to N. However, the above master equation is only valid in regimes where $\langle a_\nu^\dagger a_\nu \rangle \ll N$, such that we cannot use it to describe the regime of boosted cooling power.

APPENDIX F: FULL COUNTING STATISTICS

The starting point for the determination of currents and their fluctuations is a generalized (or tilted) Liouvillian (or rate matrix) equation of the form

$$\dot{\rho} = \mathcal{L}(\chi)\rho, \quad \text{(F1)}$$

where ρ is the vectorized part of interest of the density matrix (this could be the complete system density matrix or just the populations of a relevant subspace) and $\mathcal{L}(\chi)$ is the matrix representing the corresponding part of the Redfield or LGKS dissipator or of the rate matrix that depends on the counting field χ. In the vectorized space, the trace is computed via $\text{Tr}\{\rho\} = \vec{1}^T \cdot \vec{\rho}$ and trace conservation then implies that $\text{Tr}\{\mathcal{L}(0)\sigma\} = 0$ for any operator σ.

The moments of the conjugate variable n to the counting field can be obtained by taking derivatives of the moment-generating function,

$$M(\chi, t) = \text{Tr}\left\{ e^{\mathcal{L}(\chi)t} \rho_0 \right\}, \quad \text{(F2)}$$

via $\langle n^\alpha \rangle_t = (-i\partial_\chi)^\alpha M(\chi, t)|_{\chi=0}$. Analogously, one may obtain cumulants from the cumulant-generating function $C(\chi, t) = \ln M(\chi, t)$ by acting with the corresponding derivatives on it. In the long-term limit and for systems with a unique stationary state, one can show that $C(\chi, t) \to \lambda(\chi)t$, where $\lambda(\chi)$ is the dominant eigenvalue of $\mathcal{L}(\chi)$ (the one with largest real part, that fulfills $\lambda(0) = 0$). We are interested in the long-term limit of the lowest two cumulants of the current, i.e., in the current $\bar{I} = \lim_{t\to\infty} d/dt \langle n \rangle_t = -i\lambda'(0)$ and the noise $\bar{S}_I = \lim_{t\to\infty} d/dt \left[\langle n^2 \rangle_t - \langle n \rangle_t^2 \right] = -\lambda''(0)$. Unfortunately, for our problems, the dominant eigenvalue is not analytically known. Second-order perturbation theory for non-Hermitian matrices is rather nontrivial [86] and for larger numbers N numerical differentiation [78] is not stable. Therefore, to compute the stationary current and noise, we use a different approach [53], derived from the counting statistics of time-dependent conductors [87]. Trace conservation implies that the stationary current can be obtained via

$$\bar{I} = -i\text{Tr}\left\{ \mathcal{L}'(0)\bar{\rho} \right\}, \quad \text{(F3)}$$

where $\bar{\rho}$ is the solution to the equation $\mathcal{L}(0)\bar{\rho} = 0$, normalized to $\text{Tr}\{\bar{\rho}\} = 1$ (i.e., the steady state). With that, we can also compute the stationary noise

$$\bar{S}_I = -\text{Tr}\left\{ \mathcal{L}''(0)\bar{\rho} \right\} - 2i\text{Tr}\left\{ \mathcal{L}'(0)\bar{\sigma} \right\}, \quad \text{(F4)}$$

where the auxiliary variable $\bar{\sigma}$ is the solution to the equation $\mathcal{L}(0)\bar{\sigma} = i\mathcal{L}'(0)\bar{\rho} + \bar{I}\bar{\rho}$, normalized to $\text{Tr}\{\bar{\sigma}\} = 0$.

APPENDIX G: TIGHT COUPLING OF ENERGY CURRENTS

The Pauli rate equation [Eq. (8)] has the form $\dot{P}_i = \sum_\nu \sum_j \left(R_{ij}^\nu P_j - R_{ji}^\nu P_i \right)$, where the P_i are the occupation probabilities of energy eigenstate i (which in our state corresponds to the state $|M; m\rangle$ of the fully symmetric sector) and $\nu \in \{c, h, w\}$ labels the reservoirs. We can split

the stationary populations into the contributions from the individual cycles that couple to state i,

$$\bar{P}_i = \sum_{\mathcal{C}} \bar{P}_i^{\mathcal{C}}, \tag{G1}$$

where, e.g., in Fig. 1(b), the corner states take part in just one cycle, states on the facets take part in three cycles, and states in the interior take part in six cycles. Then, the steady-state condition can be rewritten as

$$0 = \sum_{\mathcal{C}} \left[\sum_{v} \sum_{j} \left(R_{ij}^{v,\mathcal{C}} \bar{P}_j^{\mathcal{C}} - R_{ji}^{v,\mathcal{C}} \bar{P}_i^{\mathcal{C}} \right) \right], \tag{G2}$$

and fulfilling it for every cycle obviously fulfills the complete steady-state condition. The individual conditions for a normally oriented (+) cycle read as follows:

$$0 = \Gamma_h^{\mathcal{C}}(1+n_h)\bar{P}_2^{\mathcal{C}} + \Gamma_c^{\mathcal{C}}(1+n_c)\bar{P}_1^{\mathcal{C}} - \left(\Gamma_h^{\mathcal{C}}n_h + \Gamma_c^{\mathcal{C}}n_c \right) \bar{P}_0^{\mathcal{C}},$$
$$0 = \Gamma_w^{\mathcal{C}}(1+n_w)\bar{P}_2^{\mathcal{C}} + \Gamma_c^{\mathcal{C}}n_c\bar{P}_0^{\mathcal{C}} - \left(\Gamma_w^{\mathcal{C}}n_w + \Gamma_c^{\mathcal{C}}(1+n_c) \right) \bar{P}_1^{\mathcal{C}},$$
$$0 = \Gamma_w^{\mathcal{C}}n_w\bar{P}_1^{\mathcal{C}} + \Gamma_h^{\mathcal{C}}n_h\bar{P}_0^{\mathcal{C}} - \left(\Gamma_w^{\mathcal{C}}(1+n_w) + \Gamma_h^{\mathcal{C}}(1+n_h) \right) \bar{P}_2^{\mathcal{C}}, \tag{G3}$$

where the $\Gamma_v^{\mathcal{C}}$ are cycle dependent, as they are given by the bare Γ_v rates multiplied by the squared Clebsch-Gordan coefficients from Eq. (9). Analogous equations can be written down for the negatively oriented ($-$) cycles. A solution to these equations exists, as these are just the steady-state conditions for a single QAR (see Appendix A) without the normalization constraint.

A fully analogous decomposition applies to the energy currents,

$$\bar{I}_E^v = \sum_{ij} (E_i - E_j) R_{ij}^v \bar{P}_j$$
$$= \sum_{\mathcal{C}} \sum_{ij} (E_i - E_j) R_{ij}^{v,\mathcal{C}} \bar{P}_j^{\mathcal{C}}, \tag{G4}$$

and we obtain, for the individual currents, the cycle-resolved expressions (for positively oriented + cycles)

$$\bar{I}_E^c = \delta \sum_{\mathcal{C}} \left[\Gamma_c^{\mathcal{C}}n_c\bar{P}_0^{\mathcal{C}} - \Gamma_c^{\mathcal{C}}(1+n_c)\bar{P}_1^{\mathcal{C}} \right],$$
$$\bar{I}_E^h = \Delta \sum_{\mathcal{C}} \left[\Gamma_h^{\mathcal{C}}n_h\bar{P}_0^{\mathcal{C}} - \Gamma_h^{\mathcal{C}}(1+n_h)\bar{P}_2^{\mathcal{C}} \right], \tag{G5}$$
$$\bar{I}_E^w = (\Delta - \delta) \sum_{\mathcal{C}} \left[\Gamma_w^{\mathcal{C}}n_w\bar{P}_1^{\mathcal{C}} - \Gamma_w^{\mathcal{C}}(1+n_w)\bar{P}_2^{\mathcal{C}} \right].$$

By eliminating one of the probabilities using Eq. (G3) and comparing the terms in square brackets, we can thus confirm the tight-coupling relations given in Eq. (12). Furthermore, the cooling condition $I_E^c > 0$ then also implies

$I_E^w > 0$ and $I_E^h < 0$, such that from Eq. (G5), we obtain the conditions $n_c \bar{P}_0^{\mathcal{C}} > (1+n_c)\bar{P}_1^{\mathcal{C}}$, $(1+n_h)\bar{P}_2^{\mathcal{C}} > n_h \bar{P}_0^{\mathcal{C}}$, and $n_w \bar{P}_1^{\mathcal{C}} > (1+n_w)\bar{P}_2^{\mathcal{C}}$. Multiplying these conditions then eventually eliminates the dependence on the steady-state occupations:

$$n_c(1+n_h)n_w > (1+n_c)n_h(1+n_w), \tag{G6}$$

which is equivalent to Eq. (13). Alternatively, Eq. (13) may also be obtained from the positivity of the entropy production rate $\bar{\sigma}_i = -\sum_v \beta_v \bar{I}_E^v \geq 0$ and the tight-coupling relations between the currents. Departing from the tight-coupling limit will also alter the cooling condition [88].

APPENDIX H: STATIONARY CURRENT IN THE NONCOLLECTIVE LIMIT

In the case that the stationary state is a classical one, i.e., a product state of mixtures without coherences, $\bar{\rho} = \bigotimes_\ell \left[P_0^\ell (|0\rangle \langle 0|)_\ell + P_1^\ell (|1\rangle \langle 1|)_\ell + P_2^\ell (|2\rangle \langle 2|)_\ell \right]$, it is straightforward to see that the cooling current (cf. Sec. F),

$$\begin{aligned} I_E^c &= \Gamma_c n_c \text{Tr} \left\{ S_+^c S_-^c \bar{\rho} \right\} - \Gamma_c(1+n_c)\text{Tr} \left\{ S_-^c S_+^c \bar{\rho} \right\} \\ &= \Gamma_c n_c \sum_{ij} h_i^c h_j^{c*} \text{Tr} \left\{ (|1\rangle \langle 0|)_i (|0\rangle \langle 1|)_j \bar{\rho} \right\} \\ &\quad - \Gamma_c(1+n_c) \sum_{ij} h_i^c h_j^{c*} \text{Tr} \left\{ (|0\rangle \langle 1|)_j (|1\rangle \langle 0|)_i \bar{\rho} \right\}, \end{aligned} \tag{H1}$$

will be additive in the number of qutrits. For such a steady state, in the above formula only the terms with $i = j$ can contribute under the trace, such that for $\left| h_i^c \right|^2 = 1$ (cf. the red symbols in Fig. 2), the current would be linear in the number of qutrits N. On the contrary, a superlinear scaling of the current indicates a deviation from this classical limit.

Numerically, we find that for $h_i^v = e^{i\varphi_i^v}$ as considered in the main text, the stationary state of Eq. (6) is close to the product state

$$\bar{\rho} \approx \bigotimes_\ell \left[P_0 (|0\rangle \langle 0|)_\ell + P_1 (|1\rangle \langle 1|)_\ell + P_2 (|2\rangle \langle 2|)_\ell \right], \tag{H2}$$

with normalized probabilities $P_0 + P_1 + P_2 = 1$ corresponding to the steady-state solution of a single QAR. Thus, we can link the near-linear scaling of the cooling current, which is what we observe in Fig. 2 (red symbols and dashed red line), to the near-product form of the stationary state, which would also be obtained for completely independent qutrits.

[1] M. A. Nielsen and I. L. Chuang, *Quantum Computation and Quantum Information* (Cambridge University Press, Cambridge, 2000).

[2] H.-P. Breuer and F. Petruccione, *The Theory of Open Quantum Systems* (Oxford University Press, Oxford, 2002).

[3] R. Alicki, The quantum open system as a model of the heat engine, J. Phys. A: Math. Gen. **12,** L103 (1979).

[4] F. Binder, L. A. Correa, C. Gogolin, J. Anders, and G. Adesso, editors. *Thermodynamics in the Quantum Regime—Fundamental Aspects and New Directions*, vol. 195 of *Fundamental Theories of Physics* (Springer, Cham, 2019). ISBN 978-3-319-99046-0.

[5] M. O. Scully, M. S. Zubairy, G. S. Agarwal, and H. Walther, Extracting work from a single heat bath via vanishing quantum coherence, Science **299,** 862 (2003).

[6] J. Jaramillo, M. Beau, and A. del Campo, Quantum supremacy of many-particle thermal machines, New J. Phys. **18,** 075019 (2016).

[7] C. L. Latune, I. Sinayskiy, and F. Petruccione, Quantum coherence, many-body correlations, and non-thermal effects for autonomous thermal machines, Sci. Rep. **9,** 3191 (2019).

[8] N. M. Myers, O. Abah, and S. Deffner, Quantum thermodynamic devices: From theoretical proposals to experimental reality, AVS Quantum Sci. **4,** 027101 (2022).

[9] R. H. Dicke, Coherence in spontaneous radiation processes, Phys. Rev. **93,** 99 (1954).

[10] M. Gross and S. Haroche, Superradiance: An essay on the theory of collective spontaneous emission, Phys. Rep. **93,** 301 (1982).

[11] M. G. Benedict, A. M. Ermolaev, V. A. Malyshev, I. V. Sokolov, and E. D. Trifonov, *Super-Radiance—Multiatomic Coherent Emission* (IOP Publishing, Bristol, 1996).

[12] D. Ferraro, M. Campisi, G. M. Andolina, V. Pellegrini, and M. Polini, High-Power Collective Charging of a Solid-State Quantum Battery, Phys. Rev. Lett. **120,** 117702 (2018).

[13] F. Mayo and A. J. Roncaglia, Collective effects and quantum coherence in dissipative charging of quantum batteries, Phys. Rev. A **105,** 062203 (2022).

[14] Y. Ueki, S. Kamimura, Y. Matsuzaki, K. Yoshida, and Y. Tokura, Quantum battery based on superabsorption, J. Phys. Soc. Jpn **91,** 124002 (2022).

[15] A. U. C. Hardal and O. E. Müstecaplıoğlu, Superradiant quantum heat engine, Sci. Rep. **5,** 12953 (2015).

[16] R. Uzdin, Coherence-Induced Reversibility and Collective Operation of Quantum Heat Machines via Coherence Recycling, Phys. Rev. Appl. **6,** 024004 (2016).

[17] S. Çakmak, F. Altintas, and Ö. E. Müstecaplıoğlu, Lipkin-Meshkov-Glick model in a quantum Otto cycle, Eur. Phys. J. Plus **131,** 197 (2016).

[18] W. Niedenzu and G. Kurizki, Cooperative many-body enhancement of quantum thermal machine power, New J. Phys. **20,** 113038 (2018).

[19] D. Gelbwaser-Klimovsky, W. Kopylov, and G. Schaller, Cooperative efficiency boost for quantum heat engines, Phys. Rev. A **99,** 022129 (2019).

[20] M. Kloc, P. Cejnar, and G. Schaller, Collective performance of a finite-time quantum Otto cycle, Phys. Rev. E **100,** 042126 (2019).

[21] G. Watanabe, B. P. Venkatesh, P. Talkner, M.-J. Hwang, and A. del Campo, Quantum Statistical Enhancement of the Collective Performance of Multiple Bosonic Engines, Phys. Rev. Lett. **124,** 210603 (2020).

[22] S. Kamimura, H. Hakoshima, Y. Matsuzaki, K. Yoshida, and Y. Tokura, Quantum-Enhanced Heat Engine Based on Superabsorption, Phys. Rev. Lett. **128,** 180602 (2022).

[23] L. da Silva Souza, G. Manzano, R. Fazio, and F. Iemini, Collective effects on the performance and stability of quantum heat engines, Phys. Rev. E **106,** 014143 (2022).

[24] T. D. Kieu, The Second Law, Maxwell's Demon, and Work Derivable from Quantum Heat Engines, Phys. Rev. Lett. **93,** 140403 (2004).

[25] R. Kosloff and Y. Rezek, The quantum harmonic Otto cycle, Entropy **19,** 136 (2017).

[26] J. Roßnagel, S. T. Dawkins, K. N. Tolazzi, O. Abah, E. Lutz, F. Schmidt-Kaler, and K. Singer, A single-atom heat engine, Science **352,** 325 (2016).

[27] G. Marchegiani, P. Virtanen, F. Giazotto, and M. Campisi, Self-Oscillating Josephson Quantum Heat Engine, Phys. Rev. Appl. **6,** 054014 (2016).

[28] S. Seah, S. Nimmrichter, and V. Scarani, Work production of quantum rotor engines, New J. Phys. **20,** 043045 (2018).

[29] R. Alicki, D. Gelbwaser-Klimovsky, A. Jenkins, and E. von Hauff, Dynamical theory for the battery's electromotive force, Phys. Chem. Chem. Phys. **23,** 9428 (2021).

[30] P. Strasberg, C. W. Wächtler, and G. Schaller, Autonomous Implementation of Thermodynamic Cycles at the Nanoscale, Phys. Rev. Lett. **126,** 180605 (2021).

[31] R. Kosloff and A. Levy, Quantum heat engines and refrigerators: Continuous devices, Annu. Rev. Phys. Chem. **65,** 365 (2014).

[32] J.-P. Brantut, C. Grenier, J. Meineke, D. Stadler, S. Krinner, C. Kollath, T. Esslinger, and A. Georges, A thermoelectric heat engine with ultracold atoms, Science **342,** 713 (2013).

[33] R. S. Whitney, Most Efficient Quantum Thermoelectric at Finite Power Output, Phys. Rev. Lett. **112,** 130601 (2014).

[34] B. Sothmann, R. Sánchez, and A. N. Jordan, Thermoelectric energy harvesting with quantum dots, Nanotechnology **26,** 032001 (2014).

[35] J. Um, K. E. Dorfman, and H. Park, Coherence-enhanced quantum-dot heat engine, Phys. Rev. Res. **4,** L032034 (2022).

[36] N. Linden, S. Popescu, and P. Skrzypczyk, How Small Can Thermal Machines Be? The Smallest Possible Refrigerator, Phys. Rev. Lett. **105,** 130401 (2010).

[37] A. Levy and R. Kosloff, Quantum Absorption Refrigerator, Phys. Rev. Lett. **108,** 070604 (2012).

[38] G. Manzano, G.-L. Giorgi, R. Fazio, and R. Zambrini, Boosting the performance of small autonomous refrigerators via common environmental effects, New J. Phys. **21,** 123026 (2019).

[39] M. T. Mitchison, M. Huber, J. Prior, M. P. Woods, and M. B. Plenio, Realising a quantum absorption refrigerator with an atom-cavity system, Quantum Sci. Technol. **1,** 015001 (2016).

[40] P. A. Erdman, B. Bhandari, R. Fazio, J. P. Pekola, and F. Taddei, Absorption refrigerators based on Coulomb-coupled single-electron systems, Phys. Rev. B **98,** 045433 (2018).

[41] M. T. Mitchison and P. P. Potts, Physical implementations of quantum absorption refrigerators. In F. Binder,

L. A. Correa, C. Gogolin, J. Anders, and G. Adesso, editors, *Thermodynamics in the Quantum Regime*, Fundamental Theories of Physics, chap. 6 (Springer, Cham, 2019), p. 149.

[42] G. Maslennikov, S. Ding, R. Hablützel, J. Gan, A. Roulet, S. Nimmrichter, J. Dai, V. Scarani, and D. Matsukevich, Quantum absorption refrigerator with trapped ions, Nat. Commun. **10,** 202 (2019).

[43] I. D. Leroux, M. H. Schleier-Smith, and V. Vuletić, Implementation of Cavity Squeezing of a Collective Atomic Spin, Phys. Rev. Lett. **104,** 073602 (2010).

[44] M. H. Schleier-Smith, I. D. Leroux, and V. Vuletić, Squeezing the collective spin of a dilute atomic ensemble by cavity feedback, Phys. Rev. A **81,** 021804 (2010).

[45] E. G. Dalla Torre, J. Otterbach, E. Demler, V. Vuletic, and M. D. Lukin, Dissipative Preparation of Spin Squeezed Atomic Ensembles in a Steady State, Phys. Rev. Lett. **110,** 120402 (2013).

[46] M. Kloc, K. Meier, K. Hadjikyriakos, and G. Schaller, Superradiant Many-Qubit Absorption Refrigerator, Phys. Rev. Appl. **16,** 044061 (2021).

[47] X. Wang and K. Mølmer, Pairwise entanglement in symmetric multi-qubit systems, Eur. Phys. J. D **18,** 385 (2002).

[48] B. Yadin, B. Morris, and K. Brandner, Thermodynamics of permutation-invariant quantum many-body systems: A group-theoretical framework, arXiv:2206.12639 (2022).

[49] P. Nataf and C. Ciuti, No-go theorem for superradiant quantum phase transitions in cavity QED and counter-example in circuit QED, Nat. Commun. **72,** 1 (2010).

[50] A. G. Redfield, *The Theory of Relaxation Processes*, edited by J. S. Waugh (Academic Press, New York, 1965), p. 1.

[51] J. Thingna, J.-S. Wang, and P. Hänggi, Generalized Gibbs state with modified Redfield solution: Exact agreement up to second order, J. Chem. Phys. **136,** 194110 (2012).

[52] R. Hartmann and W. T. Strunz, Accuracy assessment of perturbative master equations: Embracing nonpositivity, Phys. Rev. A **101,** 012103 (2020).

[53] G. T. Landi, D. Poletti, and G. Schaller, Nonequilibrium boundary-driven quantum systems: Models, methods, and properties, Rev. Mod. Phys. **94,** 045006 (2022).

[54] G. Lindblad, On the generators of quantum dynamical semigroups, Commun. Math. Phys. **48,** 119 (1976).

[55] V. Gorini, A. Kossakowski, and E. C. G. Sudarshan, Completely positive dynamical semigroups of *n*-level systems, J. Math. Phys. **17,** 821 (1976).

[56] G. Schaller, *Open Quantum Systems Far from Equilibrium*, Lecture Notes in Physics Vol. 881 (Springer, Cham, 2014).

[57] J. Schnakenberg, Network theory of microscopic and macroscopic behavior of master equation systems, Rev. Mod. Phys. **48,** 571 (1976).

[58] G. S. Agarwal, Open quantum Markovian systems and the microreversibility, Zeitschrift für Physik A: Hadrons and Nuclei **258,** 409 (1973).

[59] M. Esposito, Stochastic thermodynamics under coarse graining, Phys. Rev. E **85,** 041125 (2012).

[60] M. Vogl, G. Schaller, and T. Brandes, Counting statistics of collective photon transmissions, Ann. Phys. (N.Y.) **326,** 2827 (2011).

[61] A. C. Barato and U. Seifert, Thermodynamic Uncertainty Relation for Biomolecular Processes, Phys. Rev. Lett. **114,** 158101 (2015).

[62] P. Pietzonka, A. C. Barato, and U. Seifert, Universal bounds on current fluctuations, Phys. Rev. E **93,** 052145 (2016).

[63] T. R. Gingrich, J. M. Horowitz, N. Perunov, and J. L. England, Dissipation Bounds All Steady-State Current Fluctuations, Phys. Rev. Lett. **116,** 120601 (2016).

[64] S. Saryal, M. Gerry, I. Khait, D. Segal, and B. K. Agarwalla, Universal Bounds on Fluctuations in Continuous Thermal Machines, Phys. Rev. Lett. **127,** 190603 (2021).

[65] S. Mohanta, S. Saryal, and B. K. Agarwalla, Universal bounds on cooling power and cooling efficiency for autonomous absorption refrigerators, Phys. Rev. E **105,** 034127 (2022).

[66] M. Gerry, N. Kalantar, and D. Segal, Bounds on fluctuations for ensembles of quantum thermal machines, J. Phys. A: Math. Theor. **55,** 104005 (2022).

[67] A. A. S. Kalaee and A. Wacker, Positivity of entropy production for the three-level maser, Phys. Rev. A **103,** 012202 (2021).

[68] A. A. S. Kalaee, A. Wacker, and P. P. Potts, Violating the thermodynamic uncertainty relation in the three-level maser, Phys. Rev. E **104,** L012103 (2021).

[69] N. Jaseem, S. Vinjanampathy, and V. Mukherjee, Quadratic enhancement in the reliability of collective quantum engines. arXiv:2208.04250 (2022).

[70] V. Holubec and T. Novotný, Effects of noise-induced coherence on the fluctuations of current in quantum absorption refrigerators, J. Chem. Phys. **151,** 044108 (2019).

[71] A. Mu, B. K. Agarwalla, G. Schaller, and D. Segal, Qubit absorption refrigerator at strong coupling, New J. Phys. **19,** 123034 (2017).

[72] S. Restrepo, J. Cerrillo, P. Strasberg, and G. Schaller, From quantum heat engines to laser cooling: Floquet theory beyond the Born-Markov approximation, New J. Phys. **20,** 053063 (2018).

[73] D. Segal, Current fluctuations in quantum absorption refrigerators, Phys. Rev. E **97,** 052145 (2018).

[74] M. Gegg and M. Richter, PSIQUASP—a library for efficient computation of symmetric open quantum systems, Sci. Rep. **7,** 16304 (2017).

[75] R. E. F. Silva and J. Feist, Permutational symmetry for identical multilevel systems: A second-quantized approach, Phys. Rev. A **105,** 043704 (2022).

[76] M. Hayn, C. Emary, and T. Brandes, Phase transitions and dark-state physics in two-color superradiance, Phys. Rev. A **84,** 053856 (2011).

[77] A. Piñeiro Orioli, J. K. Thompson, and A. M. Rey, Emergent Dark States from Superradiant Dynamics in Multilevel Atoms in a Cavity, Phys. Rev. X **12,** 011054 (2022).

[78] J. Liu and D. Segal, Coherences and the thermodynamic uncertainty relation: Insights from quantum absorption refrigerators, Phys. Rev. E **103,** 032138 (2021).

[79] M. Esposito, U. Harbola, and S. Mukamel, Nonequilibrium fluctuations, fluctuation theorems, and counting statistics in quantum systems, Rev. Mod. Phys. **81,** 1665 (2009).

[80] J. Dalibard and C. Cohen-Tannoudji, Laser cooling below the Doppler limit by polarization gradients: Simple theoretical models, J. Opt. Soc. Am. B **6,** 2023 (1989).

[81] G. Schaller, F. Queisser, N. Szpak, J. König, and R. Schützhold, Environment-induced decay dynamics of

antiferromagnetic order in Mott-Hubbard systems, Phys. Rev. B **105**, 115139 (2022).

[82] H. Spohn, Entropy production for quantum dynamical semigroups, J. Math. Phys. **19**, 1227 (1978).

[83] S. Pigolotti and A. Vulpiani, Coarse graining of master equations with fast and slow states, J. Chem. Phys. **128**, 154114 (2008).

[84] C. Providência, J. da Providência, Y. Tsue, and M. Yamamura, Boson realization of the $su(3)$-algebra. II: Holstein-Primakoff representation for the Lipkin model, Prog. Theor. Phys. **115**, 155 (2006), ISSN 0033-068X,

[85] A. Klein and E. R. Marshalek, Boson realizations of Lie algebras with applications to nuclear physics, Rev. Mod. Phys. **63**, 375 (1991).

[86] C. Buth, R. Santra, and L. S. Cederbaum, Non-Hermitian Rayleigh-Schrödinger perturbation theory, Phys. Rev. A **69**, 032505 (2004).

[87] M. Benito, M. Niklas, and S. Kohler, Full-counting statistics of time-dependent conductors, Phys. Rev. B **94**, 195433 (2016).

[88] H. M. Friedman and D. Segal, Cooling condition for multilevel quantum absorption refrigerators, Phys. Rev. E **100**, 062112 (2019).